Modeling, simulation, and validation of a composite saw.

Julien Poirier
Mechanical Engineering
McGill University
Montreal, Quebec

August 2008

A thesis submitted to McGill University in partial fulfillment of the requirements of the degree of Master of Engineering.

Acknowledgments

This work would not have been possible without the support and encouragement of Prof. Peter Radzisewski, under whose supervision, I was able to pursue a topic that I felt was meaningful.

I would also like to thank the rest of the communition dynamics lab for their comradery and support, especially Suda and Simon. To Amy Lu for her editorial help. To Vincent Demers and Prof. Brailovski of ETS for their time and access to the equipment and materials at ETS. To Bebak for help with the MTS machine. To all the technicians in the mechanical engineering department. Also to David E. and Ronnie Schouela, whose prize encouraged me to continue into my Master's.

And most of all I would like to acknowledge all my friends and especially family whose support and constant encouragement helped me to finish my degree.

Table of Contents

Table of Figures

Index of Tables

Abstract

The operating speed of circular saws is limited by the natural frequencies of the saw. Current methods in industry of increasing the natural frequency of the saw include pretensioning, where tensile forces are introduced into the saw. The integration of shape memory alloys, to provide tensioning to the saw, is investigated as an alternative or complement to pretensioning. To better model the saw, a finite element model is compared to current software for steel saws, CSAW, a software program that calculates frequencies for stiffened circular saws. Using CSAW and the finite element method, the results are compared and the finite element model is validated for steel saws. The validated model is then used to simulate and test circular saw blade designs incorporating shape memory alloys. The designs are found to provide similar stability characteristics to tensioned steel saws.

Sommaire

La vitesse opérationnelle des scies circulaires est limitée par ses fréquences de vibration naturelles. La prétension, qui est l'inclusion ou l'introduction de contraintes de tension au périphérique de la scie, est une méthode couramment utilisée dans le milieu industriel qui permet de stabiliser la scie. L'intégration des alliages à mémoire de forme à la scie, qui produiront des contraintes en tension comparables à la prétension, est proposée. Un modèle d'élément fini ayant été validé en le comparant au logiciel de stabilité de scie, CSAW pour les scies d'acier, est utilisé pour faire la simulation et la validation du concept de la scie aux alliages à mémoire de forme. Nous démontrons ainsi que ce concept de scie est comparable à la méthode de pretension appliquée aux scies d'acier.

1 Introduction

This thesis investigates the design of a circular saw blade utilizing Shape Memory Alloys. The limitations on operation of a circular saw—blade stability and critical speed—are reviewed with respect to thermal stresses. A design is proposed and developed that addresses these operating limits while also addressing safety, manufacturability, and economic feasibility. A finite element model for the saw is developed and validated through the use of commercial saw software. The finite element model is then used to simulate the proposed design. The results are compared to current saw stability techniques.

1.1 The Problem of a Saw Blade

The limitations of circular saw operation can be defined as a problem of stability. A goal of the lumber industry is to produce as much quality lumber from raw timber. Wood lost to transformation is considered waste and must be disposed of by the operator, imposing a cost on production. Much of this waste is related to the thickness and trueness of the cut. (Trasher, 1977) The thickness of the cut, also referred to as kerf, is a function of the thickness of the saw and deflection of the saw blade. The trueness of the cut is a function of the blade stability and design of the teeth. (Quelch, 1977) A thin saw that is unstable might produce a thin cut but will still have significant kerf, as more material will need to be removed to achieve a finished surface. A thicker saw will be stiffer, and provide a truer cut, yet it will also produce a larger kerf loss. Saw manufacturers have been under increasing pressure to decrease the thickness of the saw, while maintaining cutting speed and quality. (Campbell, 1974)

The decrease in saw stability is a result of the decrease in natural frequency due to heating of the saw. The saw is heated at the periphery due to the cutting action. Due to the thinness of the saw and the low conductive value of the material used in saw blades, this heat is localized at the periphery of the saw, near the teeth. As a result of the uneven heating of the saw, the expansion of the material at the periphery results in large

compressive hoop stress at the periphery. These periphery hoop stresses result in greater saw instability by reducing the fundamental frequencies of the saw. (Lamb, 1921) The phenomenon is found in other industries such as turbine blades and refiner plates for pulping. (Campbell, 1925)

1.2 Economic Reasoning

The benefits obtained through improved saw blade design can be significant. (Denig, 1993) In the transformation process, a large amount of waste is produced. A significant portion of this waste is the result of the cutting width, or kerf, of the saw. (Kostiuk, 1978) Prior to the movement towards thin kerf saws evidenced in the 1980's; 20% of the raw log was transformed to sawdust, and overall less than 50% of the log was transformed into timber. (Kostiuk, 1995) The resulting waste, sawdust, from the kerf, is of little economic value beyond biomass energy. Pulp chips, and products used in oriented strand boards (OSB) are taken from remnants of timber, or raw logs themselves. (Trasher, 1977, Kostiuk, 1995) Due to the short fiber length of sawdust, its value is limited in pulping products and structural wood products. The waste produced by sawmills was once burned at the sawmill in beehive burners. Current environmental legislation has banned this practice throughout most of North America, and as a result of this, sawmill operators are often forced to pay to dispose of the sawdust. (Ministry of Environment, Lands, and Parks, 2003) The problem is compounded with small sawmills, as demand for process heat is not sufficient to make biomass heat generation on-site a viable option for the waste. As a by-product of production, supply of sawdust is dependant upon the health of the forestry sector, increasing operating costs for biomass energy operations due to the uncertainty of biomass supply. (British Columbia Energy Council, 1994)

Existing kerf reduction methods have been used to various successes and adoption rates. One is the introduction of band saws. This has been extensively used in large log large processing sites such as those found in Coastal British Columbia, or in new "super mills" found in the Lodgepole pine growing regions of British Columbia. (Ministry of Environment, Lands, and Parks, 2003) The bandsaw's drawbacks are the large initial

capital investment and higher maintenance costs. These costs limit the band saw's application to large operations. (Kostiuk, 1978) Many medium-sized mills use gang saws—a machine with several circular saws fixed to one arbour— that cuts a log into several boards in one pass. These machines are found in many of the regions where log size is consistent, such as the boreal forest, and production consists of studs and dimensional lumber. Small mill operators often run with a single circular saw. This is quite common in the Southern United States where private landholders will log and mill on site. (King, 1977)

For circular saws, various techniques have been used to decrease kerf losses. The primary technique involves tensioning of the saw. By inducing tension through the deformation of an inner radius of the saw, it reduces the compressive stresses caused by heating, this is further elaborated upon in section 2.5. This results in a stiffer saw when used at operating speed.

Guides are also extensively used to increase the saw stiffness. (Kostiuk, 1995) Forintek, a public-private partnership for the development of forest technology in Canada, developed and marketed guide technology to Canadian lumber producers as part of the shift towards thin-kerf saws. (Campbell, R., 1974) Most operations, except for small owner-operators, use guided saws when using circular saws. The guides perform both a stiffening action and a dampening action. Less used techniques include: running the saw at supercritical speeds, heat induction (Brdicko, 1981), and the use of weights at the collar. (Kirbach, 1989)

Heat stiffening is accomplished by heating the saw near the inner radius. This reduces or eliminates the heat gradient in the saw along the radius, keeping the saw in a neutral state. (Mote, 1981) Automated techniques for this were investigated, with the heating supplied by induction. (Brdicko, 1981) The technique has not been adopted in industry.

There have been attempts to control the uneven heating through cooling of the saw. This technique has its drawbacks. The primary one being that of the use of liquid, which

results in the formation of pulp from the sawdust and liquid, and can cause damage to the machinery. (Campbell, 1974)

1.3 Design Proposal

Logs can vary as much from tip to trunk as they can from log to log. Additionally seasonal changes in log temperature affect production mainly due to heat transfer issues. A saw that can maintain a constant kerf over such variation in log characteristics would be an asset to sawyers—saw operators—and sawmill operators.

Since increased operating speed and temperature are interrelated, when sawyers seek to operate a saw a fast as possible to increase feed rates, it results in increased temperatures. A drawback of high saw speeds is the increase in temperature is at the periphery of the saw, which lowers the critical speed. As the saw operates closer to critical speed, it will result in instability, increased kerf, and possibly disk failure.

A saw that is stable through all temperature ranges as proposed allows the manufacturer to produce a thinner saw that will be of equal stability to a thicker saw. By doing so, they can reduce kerf, while maintaining the production speeds.

The goal of this thesis is to investigate techniques in which shape memory alloys (SMA) can be used for the purpose of countering the instability of the saw due to heating. Through the use of SMA, the investigator proposes to produce a saw with the following potential benefits:

i. Increased operating speed and temperature.
ii. Decreased kerf.
iii. Decreased thickness of the saw.
iv. Increased range in which the saw is operating in optimum conditions.

The new saw's design will attempt to produce the above benefits while remaining manufacturable. In order to meet the stated goal of the thesis, the following objectives must be met:

i. Define the theoretical aspects governing saw design and operation.
ii. Address saw design issues including manufacturability, safety, performance and economic viability.
iii. Define analysis specifications.
iv. Outline and discuss simulation results.

2 Theory

To accurately design the saw, the problem of unstable saw blades is reviewed and explained. The effects of thermal stresses upon the saw are such to lower the critical speed of the saw and increase saw instability. The mechanics of shape memory alloys are also outlined.

2.1 Temperature of Spinning Disks

A saw blade is heated at the periphery of the disk, $\mathbf{r_b}$ (see Figure 2-1), by the cutting action and friction between the sides of the saw and the workpiece. As the width of the teeth on saw blades is larger than the width of the disk, little friction should occur between the disk and the workpiece. Due to vibration and the presence of sawdust, there is still however some friction that heats the saw. This is the only source of heat on the disk. Dissipation of this heat is due to convective cooling along the surface of the saw and heat energy carried with the evacuated sawdust. Some convection also occurs along the surfaces of the clamp. Very little heat escapes from the saw onto the arbour. (Mote, 1966) A hot arbour is a sign of bearing failure or other machine troubles. (Thrasher, 1977) At the arbour, the saw is assumed to have the same temperature as the surroundings. (Figure 2-3)

The disk used throughout the thesis is of 300 mm radius, **b**=300mm. (Figure 2-1)

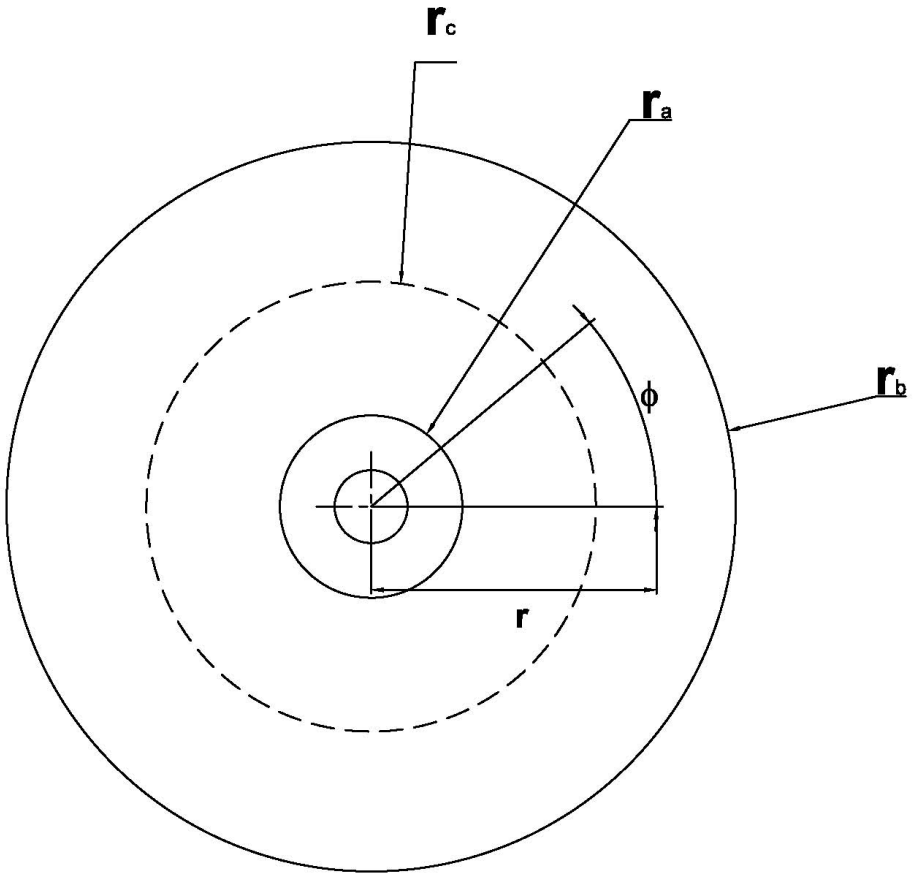

Figure 2-1 Diagram of disk with non-dimensional measurements. The dimensional measurements are obtained by dividing by the radius, b.

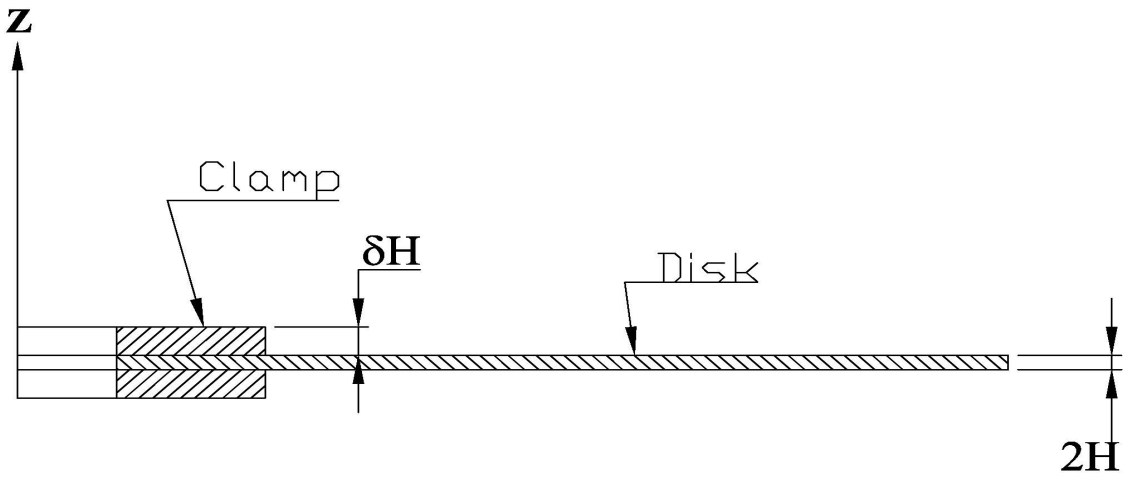

Figure 2-2 Diagram of disk from side with non-dimensional measurements.

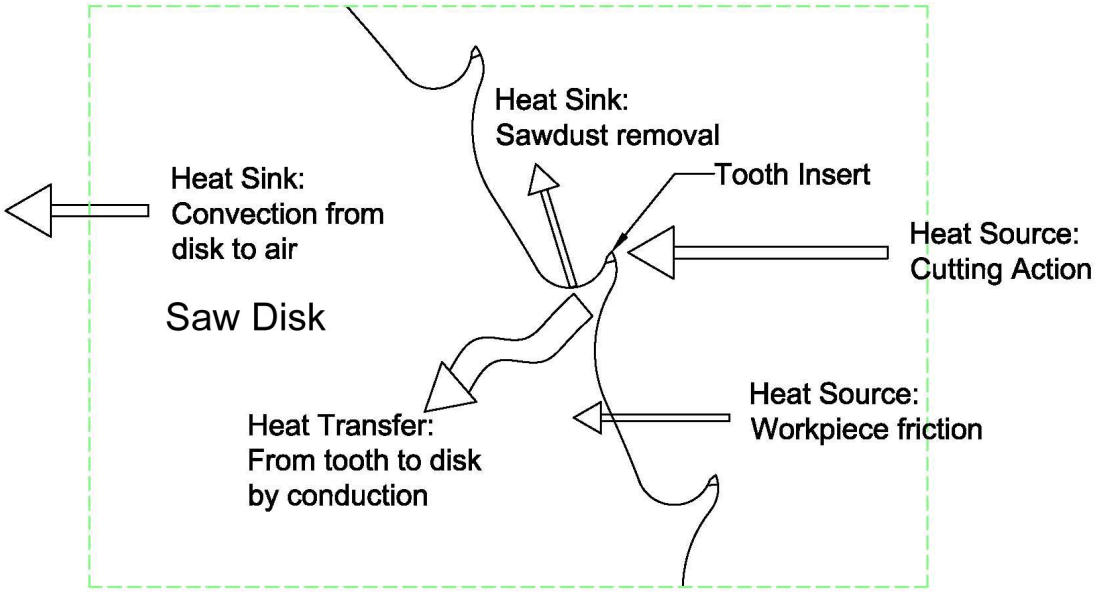

Figure 2-3 Schematic of heat transfer within a disk.

If one takes a saw tooth as a control volume, then the heat transfer can be described as illustrated in Figure 2-4. The saw tooth is subject to heating from the friction with the work piece and from the cutting action. The saw tooth is cooled by convection, conduction, and through heat evacuated with the sawdust. The heat transfer within the saw of study can be described by the control volume in Figure 2-5. The control volume is subject to heating from conductive heat transfer within the saw and from friction with the workpiece. Heat is dissipated by convection from the sides of the saw and from conduction through the saw.

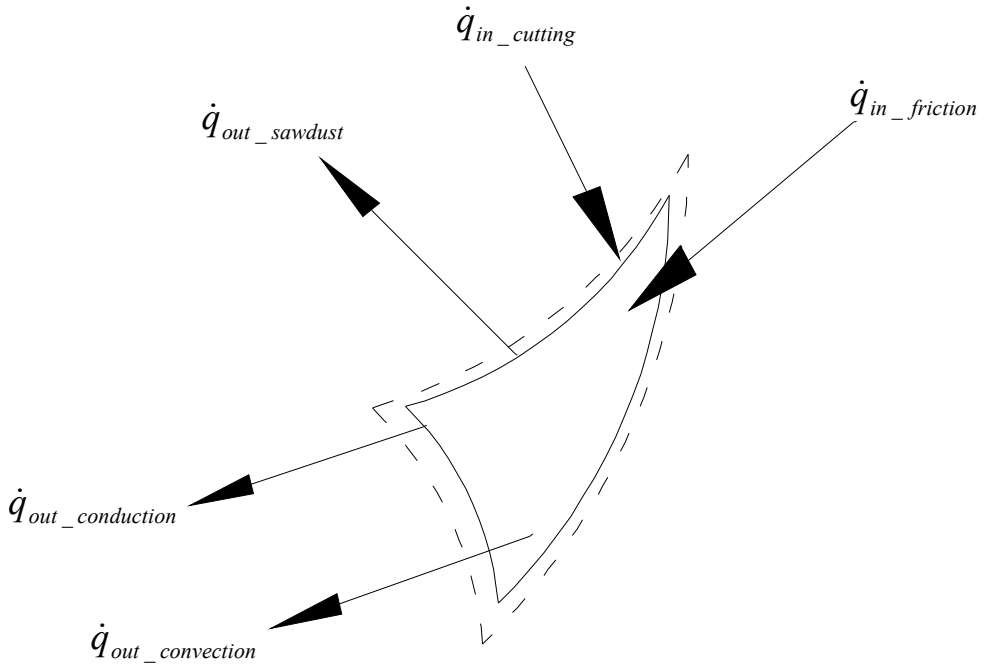

Figure 2-4 Control volume of the saw tooth.

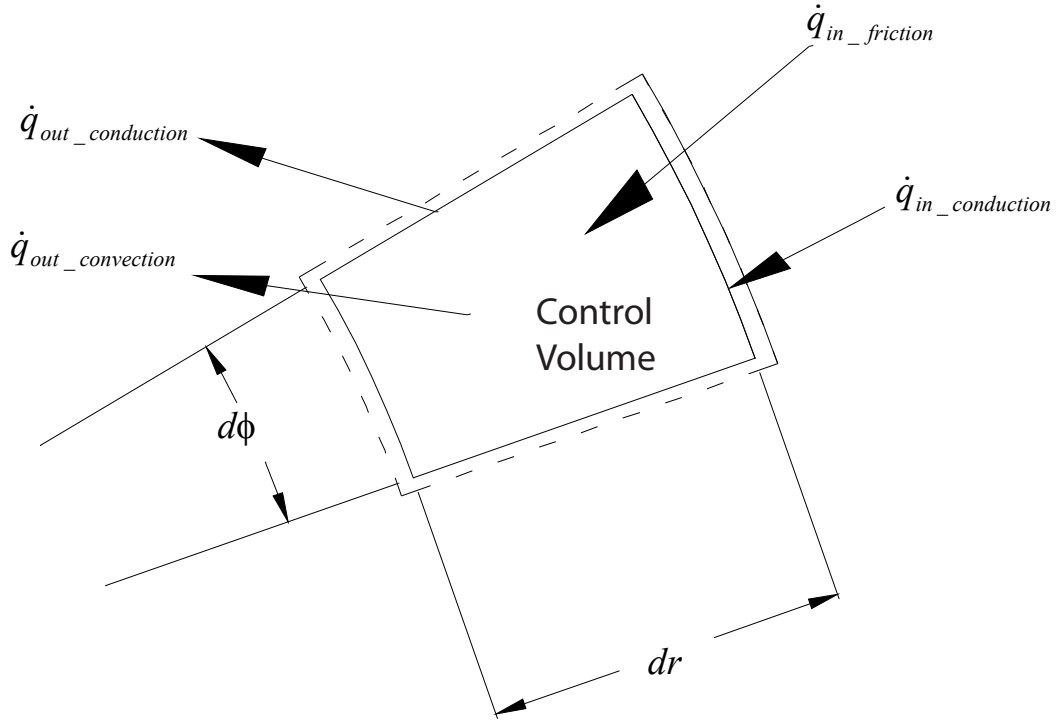

Figure 2-5 Control volume from the disk.

The temperature distribution, θ, in a disk at steady state is governed by the heat equation, Equation 2.1. (Kreith, 1978) The modified Biot number for the disk, h_{Bi}, is the ratio of conduction resistance to convection resistance.

Equation 2.1

$$\nabla^2\theta = h_{Bi}(\theta)$$

The following assumptions are made regarding the thin disk:

i. Heat doesn't conduct along the arbour.
ii. The temperature of the disk is independent of ϕ or **z**. (see Figure 2-1 and Figure 2-2**)**

The temperature of the disk can be assumed to be a function of **r** only; the thinness of the disk results in a uniform temperature in the z direction, and the heat source is equally distributed along the periphery of the saw.

Applying theses conditions to Equation 2.1, results in Bessel's Equation, Equation 2.2. (Greenburg, 1998)

Equation 2.2

$$\frac{d^2\theta}{dr^2} + \frac{1}{r}\frac{d\theta}{dr} - h_d\theta = 0$$

The general solution of Equation 2.2 is Equation 2.3. (Greenburg, 1998)

Equation 2.3

$$\theta = d_1 I_0\left(\sqrt{h_{Bi}t}\right) + d_2 K_0\left(\sqrt{h_{Bi}t}\right)$$

Where d_1 and d_2 are constants that can found by satisfying the boundary conditions. The equations for d_1 and d_2 are provided in section 2.1.2. I_n and K_n are ordinary and modified Bessel functions of n order, respectively. (Kreith, 1978)

The saw is heated at the periphery, $\mathbf{r_b}$, through the effects of friction with the workpiece and from the heat produced from cutting. As this simulation is steady state, the peripheral temperature, θ_0, at $\mathbf{r_b}$ is constant. (Mote, 1965)

The sides of the saw and the clamp transfer heat into the surroundings by convection. No heat is conducted through the arbour. (Mote, 1965)

2.1.1 Convection of a Spinning Disk and the Modified Biot Number

For the spinning disk, the convective layer consists of both laminar and turbulent regions. The division between the two is the transition radius, r_c. The convective layer of the film remains laminar for the region with a Reynolds number less than $2.5 \times 10^{5.}$ The Reynolds number, Re, for a spinning disk is found from Equation 2.4, where r is the radius, ω_0, the angular velocity, and ν is the Poisson's ratio of kinematic viscosity. (Kreith, 1978)

Equation 2.4

$$\mathrm{Re} = \frac{r^2 \omega_0}{\nu}$$

In the laminar region the convection boundary layer remains of constant thickness. (Kreith, 1978) The Nusselt number is a ratio of the convection of air compared to the conduction of air. With the Nusselt number, the coefficient of convective heat transfer of the disk can be obtained. The Nusselt number of a spinning disk in laminar flow is obtained from Equation 2.5. (Kreith, 1978)

Equation 2.5

$$Nu = .35\sqrt{\frac{r^2\omega_0}{\nu}}$$

For a Reynolds number greater than 2.5 x 10^5 the boundary layer thickens and flow becomes turbulent. In the turbulent region, heat transfer increases. (Krieth, 1978) For the spinning disk investigated, convective heat transfer results from both the turbulent and laminar convection. Equation 2.6 gives the average Nusselt number, *Nu*, for a disk with both laminar and turbulent flow. (Mote, 1967)

Equation 2.6

$$Nu = .0015\left(\frac{{r_b}^2\omega_0}{\nu}\right)^{0.8} - 100\left(\frac{r_c}{r_b}\right)^2$$

The average convective coefficient, h_{disk}, is obtained from Equation 2.7. (Kreith, 1978) The conductivity of the surrounding air is k_f. The average convective coefficient can be used for the entire disk the can be used for the disk. (Mote, 1967)

Equation 2.7

$$h_{disk} = \frac{Nu \cdot k_f}{b}$$

From the h_{disk}, the modified Biot number, h_{bi}, is found from Equation 2.8, where k_{steel} is the conductivity of the steel disk, and H is half the thickness of the disk. (Kreith, 1978)

Equation 2.8

$$h_{bi} = \frac{h_{disk}b^2}{k_{steel}H}$$

As the modified Biot number, h_{bi}, is small for the circular saw, the resistance of heat transfer between the disk and the air is much larger than the resistance of conduction along the disk, yet not sufficiently small, <.1, for consistant temperature in the **r** direction. (Mote, 1965)

2.1.2 Temperature of $\mathbf{r_a}$

To simplify the boundary conditions, the Neumann boundary condition for the center of the disk is converted into a Direchlet boundary condition. This is accomplished by finding the temperature of the disk at $\mathbf{r_a}$. (Mote, 1966) First, the convection coefficient is found for the sides, $h_{cylinder}$, and top of the clamps, h_{clamp}.

For the sides of the clamps, the Nusselt number for a spinning cylinder in air, Equation 2.9, is used to find the convective heat transfer coefficient. (Kreith, 1978)

Equation 2.9

$$Nu_{cyl} = 0.055\left(\left(78.6\sqrt{\frac{r_b^{\,2}\omega_0}{\nu}} + Gr\right)\mathrm{Pr}\right)^{\frac{7}{20}}$$

Where the Grashof number, *Gr*, is the ratio of buoyancy to viscous force and is found by Equation 2.10. (Kreith, 1978) The Prandtl number, Pr, for air is equal to 0.7. The Prandtl number is the ratio of viscous diffusion rate to thermal diffusion rate. (Kreith, 1978)

Equation 2.10

$$Gr = \frac{(\delta H)^3 \cdot 9.81 \cdot k_{air}}{T\nu^2}$$

The Nusselt number for the top of the clamps can found from Equation 2.5. The temperature at $\mathbf{r_a}$, θ_a, can found from Equation 2.11. (Mote, 1967)

Equation 2.11

$$\theta_a = \left(\frac{\theta_0 \left(I_1\left(\sqrt{h_{bi}}a\right) K_0\left(\sqrt{h_{bi}}a\right) + I_0\left(\sqrt{h_{bi}}a\right) K_1\left(\sqrt{h_{bi}}a\right) \right)}{\left(I_1\left(\sqrt{h_{bi}}a\right) K_0\left(\sqrt{h_{bi}}a\right) + I_0\left(\sqrt{h_{bi}}a\right) K_1\left(\sqrt{h_{bi}}a\right) \right) + \left(I_0\left(\sqrt{h_{bi}}a\right) K_0\left(\sqrt{h_{bi}}a\right) - I_0\left(\sqrt{h_{bi}}a\right) K_0\left(\sqrt{h_{bi}}a\right) \right) \left(\frac{k_{steel}\sqrt{\frac{h_{clamp}}{h_{bi}}}(1+\delta) I_1\left(\sqrt{h_{clamp}}a\right) I_0\left(\sqrt{h_{clamp}}a\right)}{k_{steel}} + \frac{h_{cylinder}\delta b}{k_{steel}} \right)} \right)$$

Having obtained the temperature at $\mathbf{r_a}$, the partial differential equation is well defined and the two coefficients, d_1 and d_2, can be solved. The temperature profile of the disk can now be obtained from Equation 2.3.

Figure 2-6 shows the temperature distribution of a disk with various velocities and an edge temperature of 100 °C. The edge temperature of 100 ºC is used as it was observed in laboratory test studies performed by Mote. (Mote, 1968, Ioras, 2000)

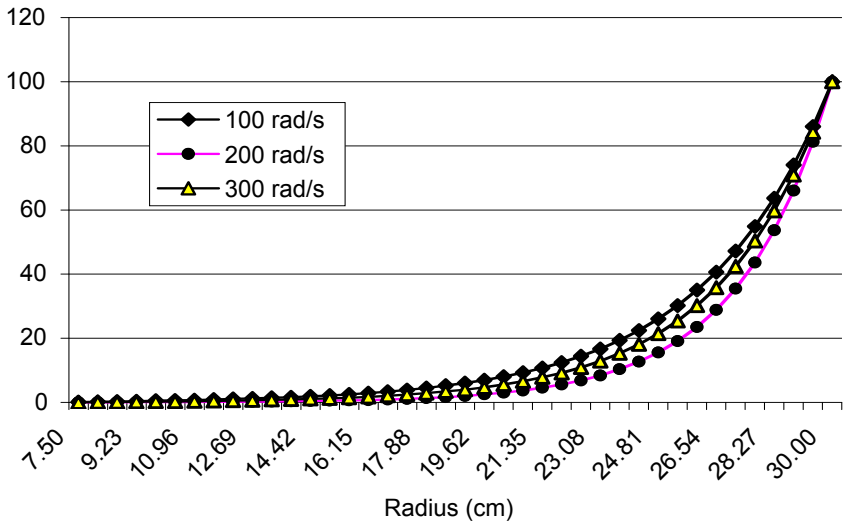

Figure 2-6 Temperature distribution with edge temperature at 100 °C.

2.1.3 Temperature of the Saw Teeth

Any heat loss from sawdust is not considered here as explained previously. For the simulations, the disk is considered to be the region just inside the disk. The teeth themselves are not modeled and when included are only included by enlarging the disk in the radial direction to an equal amount of mass. (Ioras, 2000) At the tips of the teeth temperatures of 400ºC are possible, whereas, at the junction of the teeth to the saw, the modeled disk's edge, the temperature will be closer to ¼ the tip temperature. (Mote, 1975) This is due to the larger surface area and to the heat dissipated with evacuation of the sawdust from the gullet, located in the hook next to the tooth. (Figure 2-3)

2.2 Saw Dynamics

2.2.1 Equations of Motion

The transverse vibrations of the disk are of interest, and therefore, the equation of motion will deal with the transverse displacement, **w**. For a thin disk it is assumed that the displacement does not vary in the **z** direction. The equation of motion for a stationary disk, Equation 2.12, was first solved by Kirchhoff. (Lamb, 1921)

Equation 2.12

$$\frac{D}{2H}\nabla^4 w - \frac{1}{r}\frac{\partial}{\partial r}\left(\sigma_r r \frac{\partial w}{\partial r}\right) - \frac{\sigma_\phi}{r^2}\frac{\partial^2 w}{\partial \phi^2} = \rho\frac{\partial^2 w}{\partial t^2}$$

The equation can be considered to be two uncoupled equations. First, the plate equation, Equation 2.13, and second the membrane equation,
Equation 2.14. (Timoshanko, 1925) The membrane stresses developed in Section 2.2 affect the membrane equation. The plate equation, Equation 2.13, is a function of thickness and elasticity of the plate. Time is given as t, and D is the flexural stiffness of the disk.

Equation 2.13

$$\frac{D}{2H}\nabla^4 w = \frac{\partial^2 w}{\partial t^2}$$

Equation 2.14

$$\frac{1}{r}\frac{\partial}{\partial r}\left(\sigma_r r\frac{\partial w}{\partial r}\right)+\frac{\sigma_\phi}{r^2}\frac{\partial^2 w}{\partial \phi^2}=\rho\frac{\partial^2 w}{\partial t^2}$$

The boundary conditions of the disk are described in Table 2.1. The inner boundary conditions for a spinning disk are given as Equation 2.15 through Equation 2.16.

Table 2.1 Disk mechanical boundary conditions.

Inner Boundary Conditions at $\mathbf{r_a}$	Clamped, Fixed
Outer Boundary Conditions at $\mathbf{r_b}$	Free

Equation 2.15

$$w(r_a)=0$$

Equation 2.16

$$w'(r_a)=0$$

On the inner boundary, at r equal to $\mathbf{r_a}$, the disk is clamped. (Equation 2.15 and Equation 2.16) The disk is allowed to move in the radial direction due to centrifugal stresses. The disk is assumed to exist from the origin to the outer radius yet only the region from the clamps to the outside radius is to be investigated.

At the outer radius, $\mathbf{r_b}$, the disk is free, therefore, no shearing or bending moments are present. The forces acting upon the saw from cutting are not considered in this thesis as it has been shown that the natural frequencies of the saw and the critical speed can accurately predict instability. (Mote 1967, 1975, Stakhiev 2003, Szymani, 1977a)

Equation 2.17 satisfies the shearing condition and Equation 2.18 satisfies the moment condition at the edge.

Equation 2.17

$$\frac{\partial^3 w(r_b)}{\partial r^3}+\frac{1}{r}\frac{\partial^2 w(r_b)}{\partial r^2}-\left(1+2n^2-\nu n^2\right)\frac{1}{r^2}\frac{\partial w(r_b)}{\partial r}+\frac{(3-\nu)n^2}{r^3}w(r_b)=0$$

Equation 2.18

$$\frac{\partial^2 w(r_b)}{\partial r^2}+\frac{\nu}{r}\frac{\partial w(r_b)}{\partial r}-\frac{\nu n^2}{r^2}w(r_b)=0$$

Equation 2.19, the general solution to Equation 2.12, represents the transverse displacement of the disk.

Equation 2.19

$$w=R(r)\cos(n(\phi-\phi_0))\cos(\omega_n(t-t_0)$$

When Equation 2.19 is substituted into Equation 2.18, and ϕ is set equal to ϕ_0, and t is set equal to t_0 the equation becomes an ordinary differential equation. This is the eigenvalue problem for a disk. The nodal diameter(s) of vibration are given by *n*. The solution for the eigenvalue equation will produce distinct solutions for the nodal circle modes of vibration. The eigenvalue problem has been solved exactly by Vogel and Skinner (Vogel, 1965) and can be solved using a finite difference method. (Mote, 1966)

In the saw blade problem, the influence of the teeth is not taken directly into account. Rather a distance of ½ the height of the teeth is added to radius of the disk to account for the mass of the teeth to model the saw. This technique results in discrepancies of less than 1% from a saw modeled with teeth. (Ioras, 2000)

2.3 Vibration of a Spinning disk

2.3.1 Modes of Vibration

The transverse vibrations of a circular disk vibrate along nodes that are located along diameters of the disk and along the circles of the disk. (
Figure 2-7) The largest vibrations are those of no nodal circles and low nodal diameters. It is these zero-circle vibrations that are of interest.

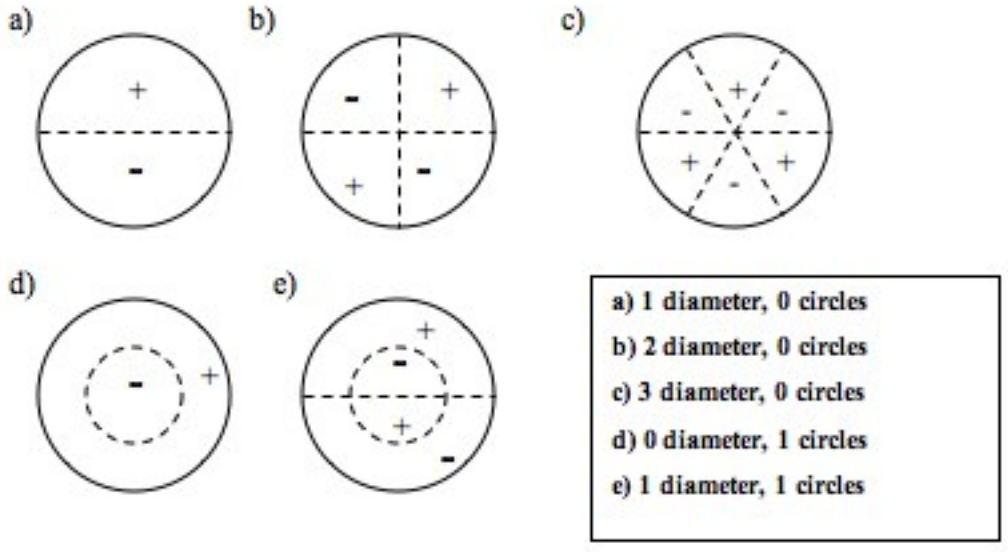

Figure 2-7 Modes of vibration for a disk.

2.3.2 Theory of Vibrations of a Spinning disk

The vibration of a stationary thin disk was first investigated and a solution proposed by Kirchhoff (Kirchhoff, 1883) Near the end of the 19th century, engineers were having difficulty explaining the failure of turbine disks. Upon further investigation it was found that these disks were failing due to excessive transverse vibrations. These transverse vibrations were being further amplified by the periodic force applied by steam nozzles upon the blades of the disk. (Campbell, 1925)

Lamb and Southwell applied the results of Kirchhoff's analysis and were able to solve for the effect of rotation on transverse vibrations of a disk. They found that the square of the vibrations of the disk, ω_n, could be approximated by the sum of the squares of the vibrations of a membrane and the vibrations of a plate. He equated the two vibrations, as shown in Equation 2.20. (Lamb, 1921) Rotation had the effect of increasing the frequency of the modes of vibration of a disk.

Equation 2.20

$$\omega_n^2 \approx \omega_b^2 + \omega_m^2$$

As the membrane stresses in the disk change, so do the modal frequencies. On large diameter, thin disks, the effect of membrane stress became predominant. Southwell and Lamb later investigated the effect clamps had on the vibration of the disk. It was found that clamping would increase the frequency of vibration of the lower modes. A large clamping radius, $\mathbf{r_c}$, would decrease the effect of membrane vibration and make the bending vibrations predominant. (Southwell, 1922).

2.3.3 Effect of Rotation and Critical Speed

The vibrations of a disk are comprised of a forward and backwards traveling wave. Theses waves travel in circular fashion around the disk. From the standpoint of an observer on the disk, the waves travel at the same velocity. However, when the disk is spinning, the rotation causes the speed of the backwards wave to decrease when observed from the viewpoint of a stationary observer. The speed of the forward wave increases as the angular velocity of the disk increases as seen from a stationary observer. As the disk reaches higher angular velocities, the backwards modal frequency will reach zero. (Campbell, 1924) To a stationary observer, this appears to be a standing wave. This results in a state similar to resonance. In this state, any axial force will induce vibration. The standing wave can be a cause of failure in spinning disks. (Szymani, 1977)

Equation 2.21

$$\omega_{cr} = \frac{\omega_n}{n}$$

The critical speed of the disk is the speed at which the backwards-modal frequency reaches zero. It is equal to the fundamental frequency of vibration divided by the number of modal diameters. (Equation 2.21) At this rotational speed, a standing wave develops and causes a state similar to resonance. The disk is unstable and failure can occur. As such, most sawmill equipment and turbines are often limited by the critical speed and are operated at up to 85% of its critical speed. (Szymani, R., 1977) As the critical speed is a function of thickness of the blade, a thicker saw is required to achieve a higher operating speed and consequently a higher throughput. This results in a larger amount of kerf loss.

Forces due to rotation have the effect of raising the frequency of vibration of all modes of vibration. The area of the disk near $\mathbf{r_b}$ is under tensile hoop stresses during rotation in the absence of heating. These rotational stresses do not cause the critical speed instability of the disk. (Szymani, R., 1976) Also of note, in the absence of rotation of the disk, a force applied along the periphery such that it would rotate about the edge of the saw, would cause instability similar to that mentioned for the rotating disk.

As the disk spins, the hoop and radial stresses increase near $\mathbf{r_a}$. At the outside edge, $\mathbf{r_b}$, the rotational radial stresses go to zero, while hoop stresses are tensile. (Dugale, 1963a) When the disk is subject to a temperature profile as outlined in section 2.1, the hoop stresses near the edge become compressive, Figure 2-8, while the radial stresses are similar to the unheated disk. The increase in the compressive hoop stresses result in a decrease in the membrane stiffness of the disk and a decrease in the modal frequencies of the two diameter and greater modes of vibration, as seen in Figure 2-9. (Mote, 1966) This effect is more pronounced for the two and three diameter modes of vibration. (Dugale, 1963b)

Mote, in 1975, found that the critical speed and stability were good indicators of kerf size. He found that the greater the fundamental frequency, the lower the amount of kerf.

By finding methods to increase the fundamental frequency, the size of the kerf can also be reduced. (Mote, 1975)

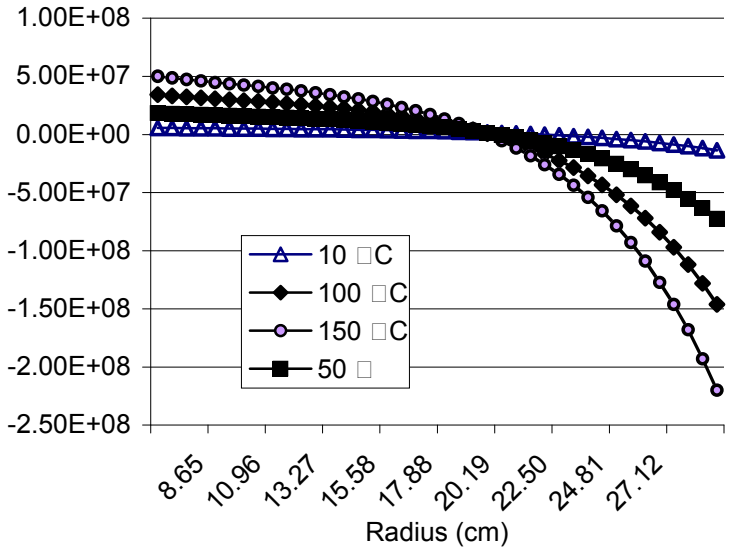

Figure 2-8 Hoop stress in a 5 mm disk rotating at 100 rad/s

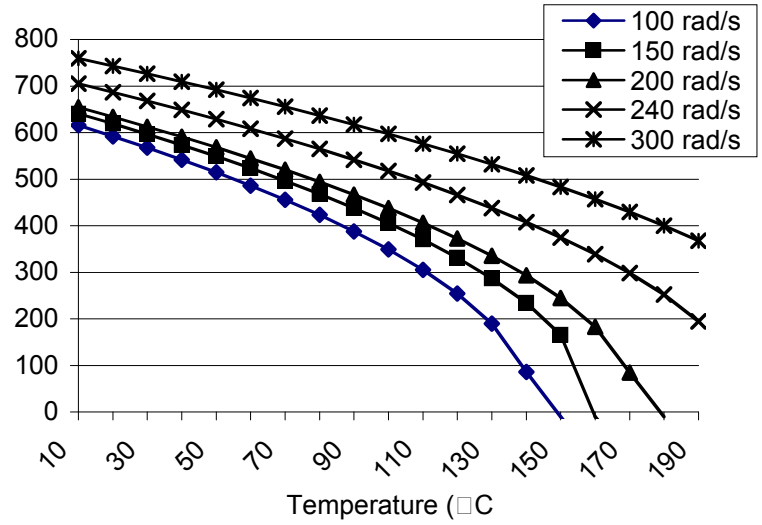

Figure 2-9 Fundamental frequency of a 5mm steel saw as seen from a rotating observer.

2.4 Roll Tensioning

To improve saw blade stability, it has been common practice in industry to tension the saw. The compressive stresses that cause the saw to become unstable are modified and countered by the tensioning. (Mote, 1965, Dugale, 1966) Tensioning is achieved by deforming the saw at a certain radius by passing the saw between two rollers as shown in Figure 2-10. As a result of the deformation, the area outside the radius that has been deformed is under tensile hoop stress. (Figure 2-11) The hoop stress is such that at low rotation speeds the disk is actually cupped. Tensioning the saw is an act that produces a saw that is optimized for specific operating conditions. (Stakhiev, 2004) The resultant stresses in an operating disk are show in Figure 2-12.

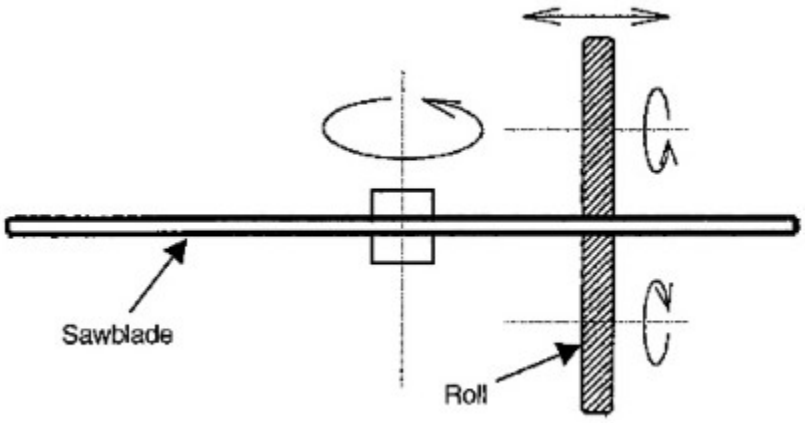

Figure 2-10 Method of roll tensioning. The disk is rotated between two rollers, which exert enough force to deform the disk. (Kuratani, 2000)

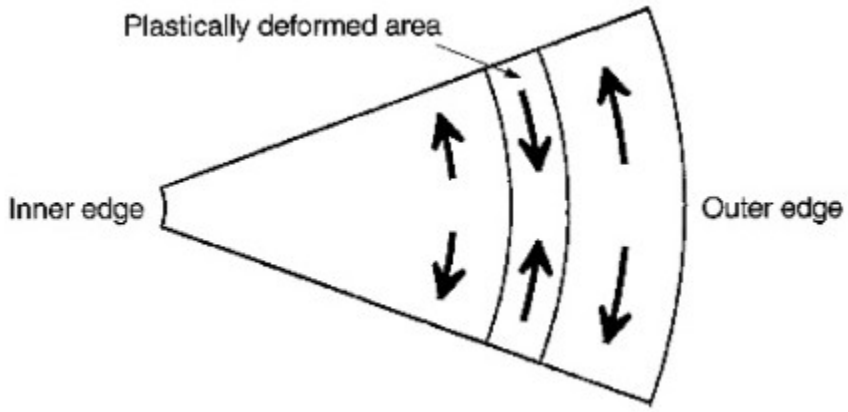

Figure 2-11 Resultant stresses in roll tensioned disk. The deformed region is under compressive stress while the regions outside the deformed area are under tensile hoop stress. (Kuratani, 2000)

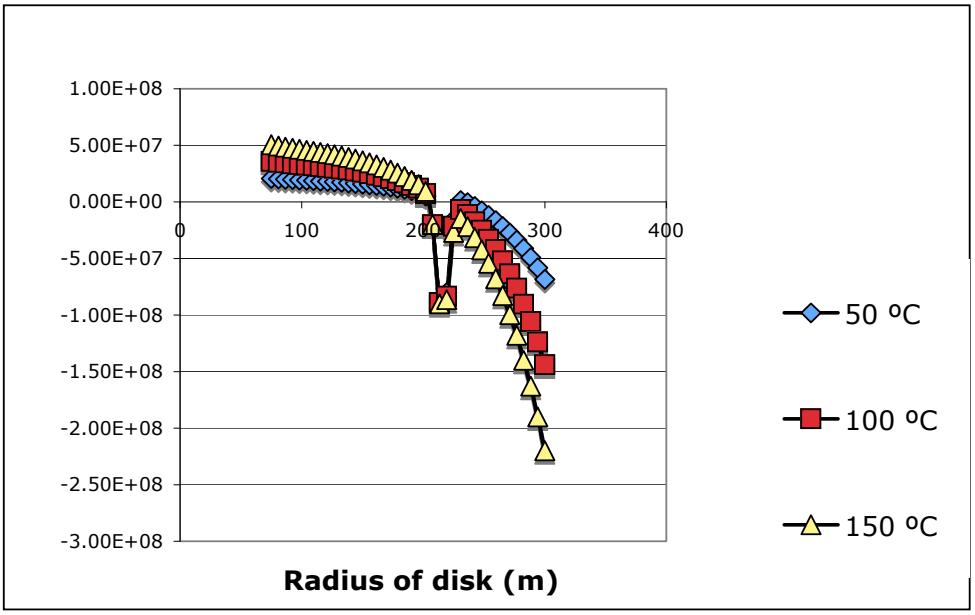

Figure 2-12 Hoop stresses obtained for 50º C tensioning temperature profile at .78 r_b.

2.5 Shape Memory Alloys

Shape memory alloys (SMA) are alloys that when heated, show the ability to revert to its original crystal structure, or phase, as well as its original shape. The two phases of concern for the shape memory effect of SMA are the lower temperature martensite phase, and the higher temperature austenite phase. By the application of heat, the material

changes phase from the martensite phase to the austenite phase. In the martensite phase the material easily deforms due to the materials atoms moving in a shear-like fashion (Ostuka, 1998). The deformation of the crystals is similar to the folding of an accordion. When the SMA is heated the process is reversed and the crystal lattice unfolds. (Hodgeson, 1999)

The phase change between austenite and martensite occurs between $\mathbf{T_{As}}$ and $\mathbf{T_{Af}}$. Figure 2-13 demonstrates the path taken from the martensite phase to the austenite phase and back to the marensite phase as the material is heated and then cooled, and the associated fraction of martensite in the material. The austenite phase shows isotropic elasticity similar to most metals. For most SMAs, the shape memory effect typically occurs during heating, although some materials can be trained for two-way shape memory, where a material after having transformed into the austenite phase will remember the deformed shape previously held in the martensite phase and revert to this shape when cooled to the martensite phase. (Otsuka, 1998) When cooled the SMA will revert to the martensite phase. $\mathbf{T_{Ms}}$ occurs at a temperature lower than $\mathbf{T_{Af}}$, and the material will only be completely in the martensite phase at a temperature lower than $\mathbf{T_{Mf}}$, which is at a temperature lower than $\mathbf{T_{Ms}}$. The percentage of each phase in the material during the phase change is proportional to the temperature. Figure 2-14 demonstrates the cycle of the shape memory effect. (Hodgeson, 1999)

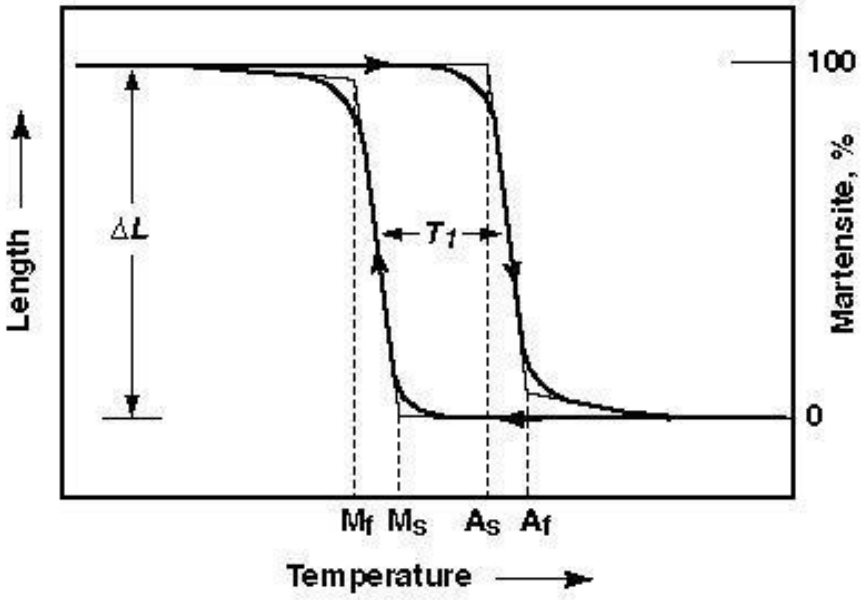

Figure 2-13 Graph showing path of phase changes in SMA. (Hodgeson, 1999)

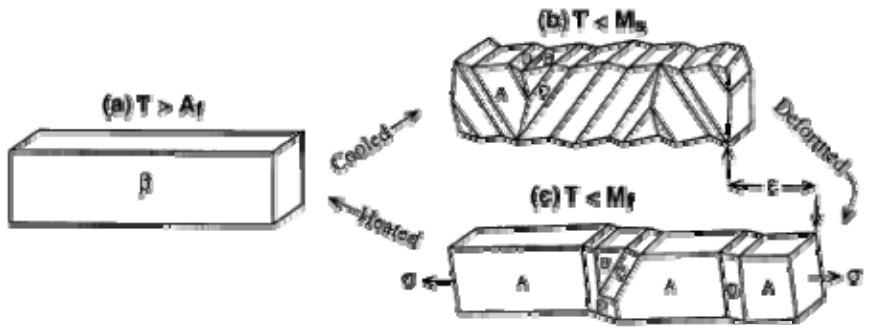

Figure 2-14 Shape Memory Effect. (Hodgson, 1999)

The two phases also demonstrate different Young's modulus. The martensite has a Young's modulus of elasticity approximately half of the austenite phase. (Ostuka, 1998)

Heating the material for a prolonged period in the desired shape causes the material to remember the shape. The temperature required is usually below the annealing temperature. (Shaw, 1995) Once the shape is memorized, the shape memory alloy will return to its memorized shape after being heated if the deformations while in the martensite phase are within 3-8%. (Hodgeson, 1999)

These properties are true of all shape memory alloys, but very evident in nickel titanium with 50% to 60% nickel. The SMA referred to in the thesis is generally nickel titanium. Specific alloys used in the analysis are elaborated upon in chapters 3 and 4. The most widely used alloy is nickel titanium, also known as NiTi or Nitinol™. Specifically for this thesis NiTi with 50% to 60% titanium, remainder nickel, is used. This alloy's properties are the most desirable amongst the class of shape memory alloys. It has high fatigue resistance, can be deformed up to 8%, and is capable of recovery stress –the stresses resultant from constraining the material during the shape memory effect– of up to 1400 MPa. (Demers, 2004)

2.5.1 Repeated Stressing of SMA

With repeated cycling of the SMA, the material's shape memory properties will decrease. As shown in Demers' work and other sources, constrained memory stresses decrease with repeated cycling. At approximately 100 cycles, the material will show near constant constraint stresses. (Demers, 2004, Shaw 1995)

Also exhibited over repeated cycling is the shifting of the transformation temperatures at which the stresses are present. This shift is largely inconsequential and less than the variance in transformation temperatures within NiTi samples of similar composition.

2.6 Summary

The stability dynamics of a circular saw blade are influenced by disk thickness, rotational speed, and temperature. The effect of temperature on the saw is a result of the cutting action, and the effect of heat is localized at the periphery. The influence of stresses in the disk due to thermal loading has large effect on the saw, including lowering the critical speed. The rotational speed of the saw in operation is limited by its critical speed, and operation of the saw near the critical speed increases saw instability.

Shape memory alloys are a class of materials that can return to a memorized shape during heating. SMA can be used in applications where heating creates a negative response. Of the SMA currently available, NiTi is the most widely available, and possesses the strongest shape memory abilities. These properties fall within the desired properties for the design in terms of: recovery stresses, fatigue strength, and temperature range.

3 Saw Design

Previous work in the design of a circular saw with integrated shape memory alloys is discussed. As part of the design process, the issues of manufacturability and safety of the saw are investigated and addressed. The use of SMA poses unique circumstances such as machining and joining, yet as explained in this chapter these challenges are surmountable with current methods. Several designs for a composite saw are advanced with different joining techniques. These designs are compared and ranked.

3.1 Previous Design

The use of SMA in a saw has been investigated in previous work. (Poirier, 2003) In that study, the SMA was incorporated into the saw in an ideal fashion. It is assumed that the NiTi is perfectly bonded to the steel disk. This design consisted of two bands of SMA sandwiching the periphery of a steel disk. (Figure 3-1) Where the bands of SMA are in contact with the disk, the disk was machined thinner so that the final composite disk is flush along its surface. (Figure 3-2) This disk was simulated using the finite element analysis program ANSYS^{TM}. The results of this design were positive, and the need for further study was apparent.

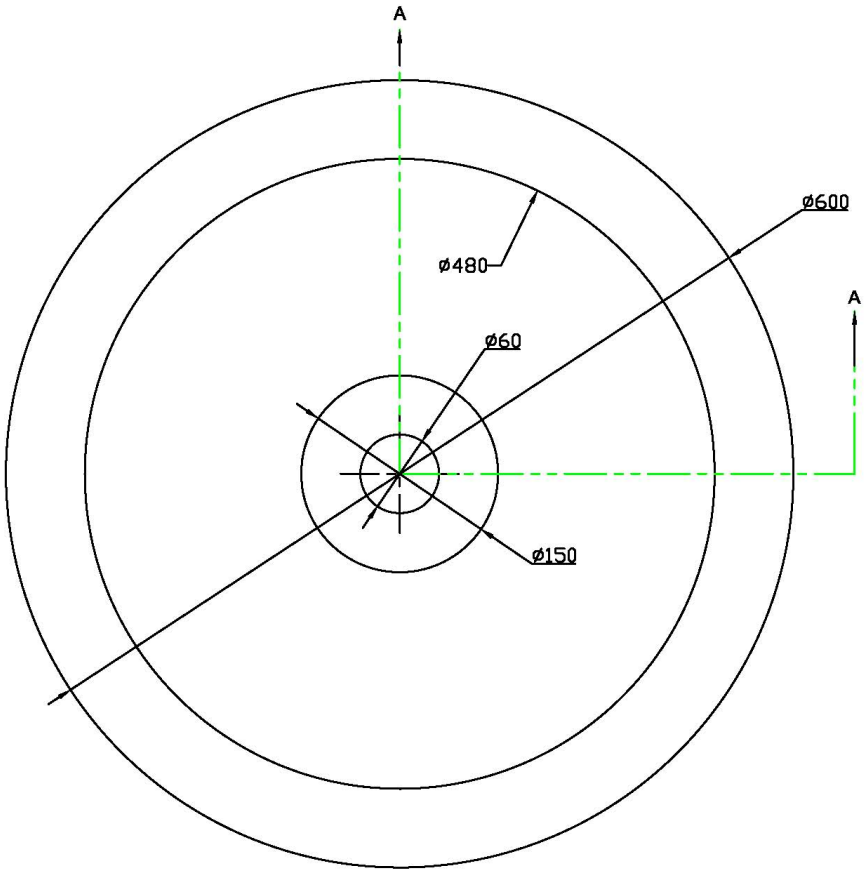

Figure 3-1 Ideal saw design, front.

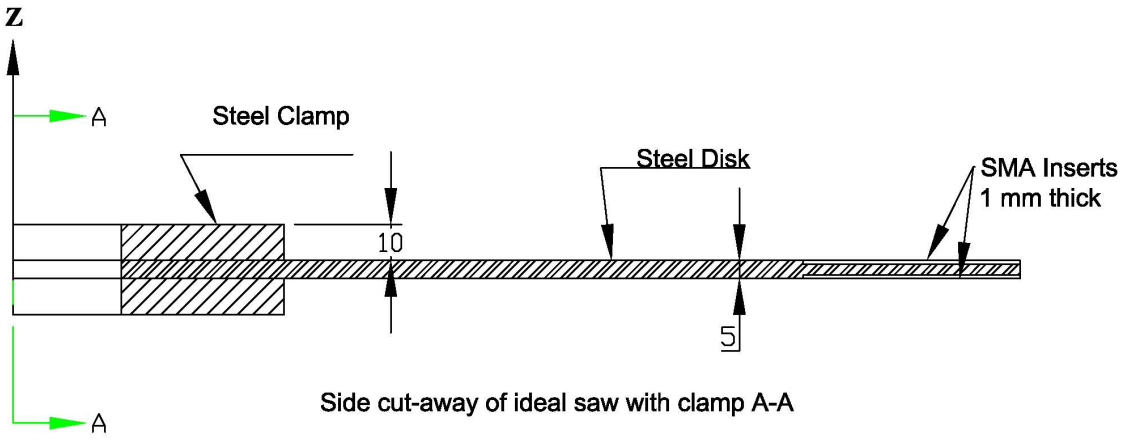

Figure 3-2 Ideal disk, side.

3.2 Manufacturing Issues

The development of a saw blade comprised of more than one part, or of materials other than steel poses challenges in terms of safety and manufacturability. These issues are addressed in the following section.

3.2.1 Disk Material

Steel continues to be used as the base material of the saw. The reasoning behind this are that the overall qualities of NiTi were inferior to steel when used as the sole material. NiTi has a lower Young's Modulus than steel in both the martensite and austenite phases and would incur larger amplitude deflections while in operation, resulting in larger kerf. For the design, the properties of the NiTi (50.4% titanium, remainder nickel) used are provided in Table 3.1, and Table 3.2. (Demers, 2004, Hodgeson 1999)

Table 3.1 NiTi properties.

Properties of NiTi	Martensite	Austenite	
Young's Modulus of Elasticity (E)	40	80	GPa
Poissons Ratio (μ)	0.3	0.3	
Density (ρ)	6450	6450	kg/m^3

Table 3.2 NiTi Phase change temperature.

Phase Change Temperature	
Austenite Start	Austenite Stop
40ºC	80ºC

The use of NiTi on the surfaces of the saw does not pose a problem in terms of durability of the material when in contact with guides or other hard materials. (Hodgeson, 1999) NiTi easily work hardens, similar to titanium, and has been used for wear resistance in other applications such as cavitation resistance, and tooling applications. (Paro, 2004)

Stainless steel was also considered due to similar stiffness properties as steel, and the possibility to be fusioned with the NiTi using intermediate materials such as refractory metals. Stainless steel saws were long avoided in the sawmill industry due to higher saw manufacturing costs and difficulty in saw maintenance; however the proliferation of computerized saw maintenance equipment and centralized saw filing operations has seen the use of stainless steel saws gain acceptance in many sawmills. (Szymani, 1986) A drawback to stainless steel is the lower yield strength compared to saw blade tool steel. These lower yield strengths pose challenges when using mechanical fastening techniques to join the SMA to the stainless steel. It has therefore not been used in the designs.

3.2.2 Safety Issues

Disk failure is a problem present with all saw blades. Sawmilling companies have adopted several measures to address this safety concern.

Enclosed Workspaces

Modern sawmills, as found in the in BC Interior lumber industry, have enclosed most moving parts. Computer automation and cameras have isolated equipment such as gang saws, trim saws, edgers and cutoff saws from the operator and surrounding workers. As such, disk failure is contained within these enclosures, decreasing the risk of workplace injuries. (Gleeson, 1977)

Furthermore, better understanding of log characteristics and machine vision has increased the effectiveness of sawing. The appropriate speeds and paths are chosen depending on the log conditions such as frozen logs, log humidity, density, size and knots. (Thrasher, 1977, Quelch 1977) Operating in optimal conditions lessens the chances of bucking and saw failure.

Saw Failure Through Striking Metallic Objects

Following protest tactics by environmentalists during the 1980's and 1990's, sawmills routinely test for metallic objects in the logs. The tactic of "spiking" the tree involved the

introduction of a nail or similar object into trees in forests where logging was controversial. Although rare, trees processed today can still contain these spikes. The danger with these metallic objects in the tree are that they are usually difficult to detect to the naked eye, and when struck with a cutting device such as a chain saw or sawmilling equipment, will cause catastrophic equipment failure, potentially injuring the operator. Metal detectors have decreased the incidents of striking a metallic object within trees in sawmills. (Williston, 1988)

Dislodged Objects

The risk of flying objects is present whenever rotating equipment is not composed of a homogeneous part. Saws often contain brazed teeth that can fail and fly off the saw at great velocity. As mentioned previously, passive safety measures such as enclosing rotating equipment has decreased the potential for injury from flying objects.

Several saw blade designs have incorporated press fitted parts. Even with these designs in use the rate of injury and death in the transformation areas of sawmill in relation to machine injuries is not significant. (Alamgir, 2006)

Other designs such as the arbor saw tensioning device, whereby the arbor was comprised of free-floating wedges which would under rotational forces press along the inside diameter, thereby increasing the disk diameter and decreasing the compressive hoop stresses. The other designs have been built and tested without a decrease in safety for the object.

Overall the design of the saw must be such that the saw continue to operate during its specified time. Catastrophic disk failure, or even small failures such as the loss of braised teeth or rivets as in the case of the composite saw's design would render the saw unmarketable. The new large operations such as Canfor's Prince George Sawmill rely on high throughput operation, and disk failures can result in interruptions of several hours, endangering the economics of such operations. As such, reliability for the prescribed hours is required.

Bucking and Critical Speed Failure

Beyond striking a metallic object or metallurgic deficiencies, catastrophic saw failure is due to the result of operating too close to the critical speed, or excess disk stresses due to heating. (Lamb, 1922) Such conditions can lead to bucking in the saw and failure, or to too large transverse disk displacement, where a saw tooth can engage too large a cut resulting in large forces in the saw and failure. (Thrasher, 1977)

By operating away from the critical speed, chance of such failure can be minimized. The transverse displacement and kerf is minimized, maximizing saw tooth efficiency and decreasing the resultant stresses in the saw from the cutting action. Chip size is also optimized increasing heat and mass transfer away from the saw.

By proposing and designing a circular saw which can adapt to differences in operating conditions such as fiber type and fiber humidity the saw can remain in this optimum operating range, decreasing the possibility of failure.

The circular saw bodies can operate in a normal mill for nearly a year. Yet teeth must be replaced or sharpened once per eight-hour shift. During such maintenance, it is possible to test and to observe the saw for failure near the inserts, and conduct repairs or replacement as required.

Saw filing and maintenance has largely been relegated to contracted out operations. The lack of filer apprentices and investment has made onsite saw maintenance rare. As such, saw-filing contractors can benefit from economies of scale when using imaging equipment to detect failures. Such techniques could be beneficial to current steel saws, preventing failure in operation from metallurgic deficiencies.

3.2.3 Manufacturing Process

The use of shape memory alloys has largely been limited to the realm of high tech industries such as aerospace (Flanges in F-14 fighters), health care (Stents for arteries), and robotics (Linear motors). Yet this material has found use in what could be considered simpler applications. Such examples are heat-regulating valves in domestic shower controls and in retractable cell phone antennas.

The choice of nickel titanium suffers from many of the manufacturing drawbacks of titanium. These drawbacks result in a manufacturing process that must be well defined to control costs. The possibility of outsourcing these processes is often limited to specialists. As such, many of the applications of NiTi are performed in a vertically integrated process. (Hodgeson, 1999)

Nickel titanium founding

Nickel titanium is often founded in vacuum induction ovens due to the need for purity and to prevent the oxidation of titanium. Other methods of founding include electron beam melting, vacuum arc melting, and plasma arc melting. (Hodgeson, 1999) After the material is founded, it is then processed into wire through rolling. The rolling process requires that the material be often annealed as hardening due to cold working quickly sets in. (Smallman, 1999) By founding the material into ingots that are better suited to the designs of the inserts in the composite saw, rolling can be kept to a minimum, and primarily for inducing the shape memory effect into the material.

Manufacturing of nickel titanium has also been performed by pressing thin sheets of pure nickel and titanium through cold rollers, where the sample is folded over and rolled over several iterations. This process can be performed through an inert gas bath rather than a vacuum. The use of this process can result in a nickel titanium product that would closely resemble the final inserts in shape, minimizing working of the product. (Otsuka, 1998)

The preparation of shape memory alloy requires that the final shape be set through heating in an oven while constrained. Such manufacturing process is very similar to the

curing of fiber and epoxy composite materials, such as carbon fiber. Such process has been commercialized in processes such as the manufacture of hockey sticks, and aerospace materials such as wings, floors, and panels. This process is readily available and widely standardized. (Smallman, 1999)

The process of deforming the material away from its memorized shape is also a process that is repeated outside the manufacture of shape memory alloys. Stamping of metal follows a similar process, and can be done in a similar economical fashion.

Machining the saw

The shape of the steel saw can be processed via current saw manufacturing techniques. The slots of the saw as well as the saw shape can be obtained through laser or water cutting as is currently done in saw manufacture facilities.

The thinning of the saw where the inserts lie can be obtained in several methods (Shackelford, 1999):

i. Electro Discharge Milling. EDM milling followed by polishing can accomplish the material removal to achieve the thinner sections where the inserts lay.
ii. Chemical Milling. The process is similar to EDM.
iii. Abrasion Milling. The use of abrasives is used to remove material rather than a cutting action as with standard machining.

Also possible is the stamping of the metal such that the area of the inserts is rendered thinner. Finishing by grinding is possible. Difficulties with jigs would be minimal as the disk material, steel, can be held with a magnetic chuck. (Shackelford, 1999)

Thin rivets

The greatest challenge towards manufacturability is that of the assembly of the saw with rivets. When working with such thin materials in a high stress condition, the possibility of failure is present through shearing thru of the rivets from the thin inserts and saw.

Extensive research and testing has been done with riveting and thin materials in the aerospace industry. The engineering thresholds are understood and well documented. This step of the manufacturing process, although challenging, can be accomplished. The design of the saw in this thesis has been made as per safety thresholds outlined in documents such as the Machinist Handbook (Oberg, 1969), and from rivet and sheet metal design tables from aerospace design works (Lindeburg, 2002, Sun, 2006). Margins of safety have been included. These margins of safety are not as large as found in typical machine design, but are larger than aerospace manufacture.

For the design, the rivet stresses are shown in Table 3.3**,** and calculated from Equation 3.1 for rivet shear stress, τ, Equation 3.2 and Equation 3.3 for tensile stress, $\sigma_{t,steel}$ in the disk between the wires and Equation 3.4 for bearing stress, σ_p. (Lindeburg, 2002, Oberg, 1969) Diameter of the rivet is given as *d*, the distance between rivets, p and force *F*. As seen in Table 3.3 the shear stress has the least amount of safety but is still within allowable limits. Bearing and tensile failure should not be a concern.

Equation 3.1

$$\tau = \frac{F}{\frac{1}{4}\pi d^2}$$

Equation 3.2

$$A_t = (p - d)2H$$

Equation 3.3

$$\sigma_{t,steel} = \frac{F}{A_t}$$

Equation 3.4

$$\sigma_p = \frac{F}{d \cdot 2H}$$

Table 3.3 Safety factors on rivets and treaded SMA.

	Allowable MPa	Designed MPa	Safety Factor
Shearing	400	200	2
Tensile	1900	27	70
Bearing	1900	64	30

In sawmilling saw design, the use of supercritical saws have been such that the margin of safety are much smaller than that found in sub critical saws that have been prevalent in the industry up to now. The supercritical saw has been adopted in high production mills. These saws although operating closer to their engineering limits, have not resulted in increased downtime or increases in injuries. (Szymani, 1984) The safety issues and mitigation proceedures have been discussed in section 3.2.2.

Cycling of the inserts could be high as a result of the quick heating and cooling cycle between each pass of the workpiece in the sawmilling process. As such, this part of the saw design would have to be properly benchmarked during testing to keep track of any weaknesses resulting from fatigue. Use of proper measurement and testing equipment would keep track of any potential failures while prototyping.

Actual prototyping of the saw was outside the purview of this thesis, and would have to be covered in future work in this subject.

3.3 Shape Memory Alloy Design Development

The development of a design involving the use of shape memory alloys requires that the shape memory effect (SME) be addressed to benefit from this phenomenon. The saw design process is looked at with relation to the SME and three saw concepts, a press-fit SMA insert saw, a threaded SMA, and a slotted insert saw, are put forward and compared against a standard saw in sections 3.3.4, 3.3.6, and 3.3.7.

3.3.1 Shape Memory Alloys Design Difficulty

Shape memory alloys pose several design challenges when it comes to manufacturing. The use of NiTi presents many of the same problems as titanium: difficult to work with, expensive foundry work and cold working, expensive machining techniques and limited ability to be welded. The hardness of the NiTi in the austenitic form is such that it can cut through mild steel. When clamping the samples of NiTi, the use of oil-hardenable steel (AISI 1080)—having a higher hardness than mild steel—was required although hardening was not. (Oberg, 1969)

3.3.2 Repeated Stressing of SMA

With repeated temperature cycling of the SMA material, the recovery stresses obtained will decrease. As shown in Demers's 2004 work and other sources, constrained memory stresses decrease with repeated cycling. At approximately 100 cycles, the recovery stress will be approximately 50% of the initial recovery stress. Also at this point, the recovery stress will remain consistent through further cycling. (Demers, 2004)

Also exhibited over repeated cycling is that the temperature at which the stresses are present will shift. This shift is largely inconsequential and smaller than the variation in transformation temperatures between samples (1-2 ºC difference). (Demers, 2004)

Most data available concerning SMA was produced using laboratory-sized samples. These samples are filament sized (diameter <1mm) and demonstrate ideal SMA properties. This can be achieved because all the cold working and tempering of the alloys is homogenous throughout the samples. As the size of the samples increase, errors are introduced in the sample: the material isn't consistently cold worked throughout, and tempering temperatures and times can vary throughout the sample.

Due to the thickness of the material, temperature distribution became a larger issue. Some parts of the material remained in the martensite phase at final change temperatures much lower than the lab samples had. Again the inconsistent working of the material led to a broader range of transformation temperatures. (Demers, 2004)

Material preparation for SMA requires that the material be stressed through cold working to achieve the desired properties. As a result of the large diameter size, this cold working is not uniform throughout the material. Some areas of the material would harden much quicker than others. This resulted in non-uniform crystals throughout the material and the properties where diminished.

After several tests it was found that maximum stresses possible the samples would be in the 400 MPa range with long-term stresses in the range of 200 MPa. These stresses are compatible with the design requirement. (Figure 3-6) They were also within the designs of the previous FEA saw as it had included significant conservative estimates, and older NiTi stress data. Since those stress results were produced, studies with cold rolled NiTi have shown higher stresses capable, up to a yield strength of 1400 MPa. Other than the change in maximum recovery stress, the material performed as predicted. The maximum recovery stress obtained was still larger than the recovery stresses required for the saw.

Other tests were performed having clamped the SMA strips, Figure 3-3, in between two steel pieces, Figure 3-4. As the samples were placed in a testing rig to measure stress produced, Figure 3-5. The results obtained were consistent with published data. (Demers, 2004)

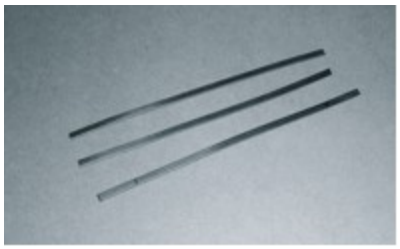

Figure 3-3 NiTi test strips.

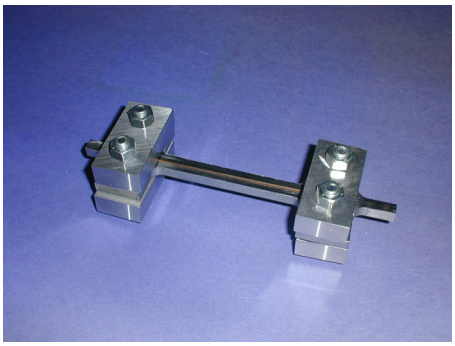

Figure 3-4 Clamp used for NiTi strips. To strips of NiTi are clamped on either side of a steel dogbone.

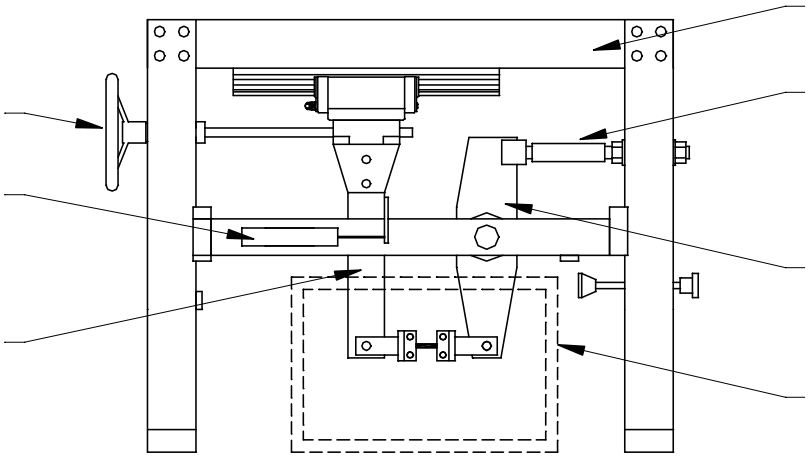

Figure 3-5 Test rig for obtaining recovery stresses. (Source ETS)

Residual stress was present in the sample after testing due to the hysteresis. After repeated cycles the stress of the material was lower as predicted with the performance of the SMA over several cycles.

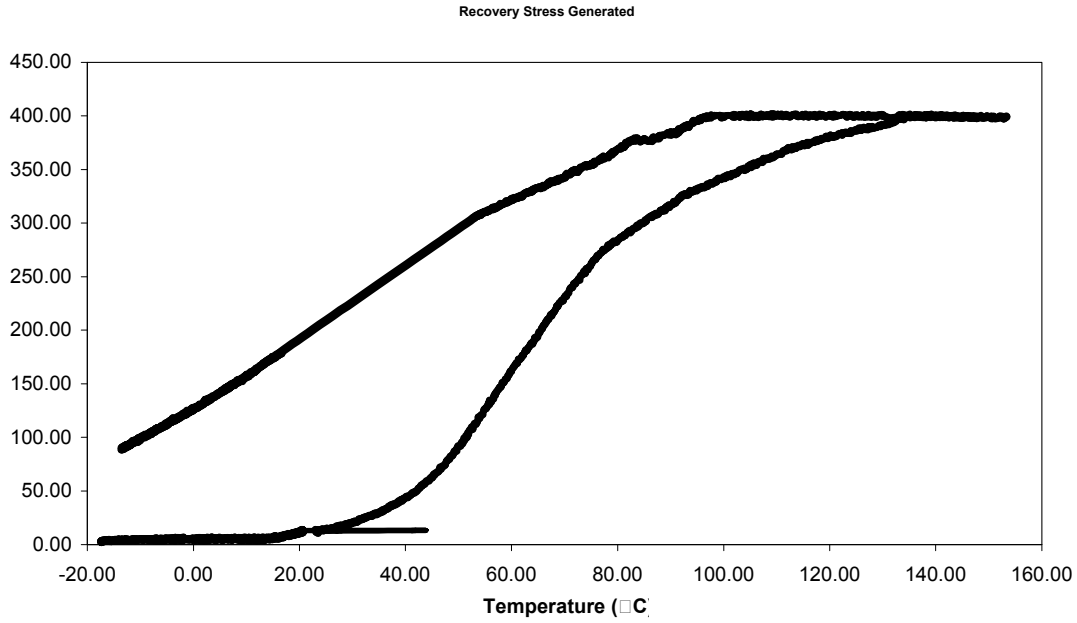

Figure 3-6 Stress generated by 1mm dia. NiTi strip. Under Heating is the lower path, and subsequent cooling is the upper path. (E=.81, anneal temp= 400ºC)

The steel thickness was such that buckling would not be a factor in the tests. The steel did expand as predicted, but its rate was delayed and the expansion was less than the rate that would have been obtained for steel alone. Heating was done at slow enough rates so that all the materials would heat evenly.

Based on the stresses involved, fatigue would not be a factor. This was based on research of both the steel and SMA by other investigators. (Eggeler, 2004) NiTi has been investigated by several authors and has been found to be able to hold its properties over 100 000 cycles, when deformed less than 2%. (Shaw, 1995, Hodgeson, 1999) As for steel, it is already extensively used in sawmilling, and design called for a disk that could perform with similar life expectancy as a currently available circular saw blade.

The shape memory property of NiTi is largely dependant upon the composition of the alloy. With NiTi, a .1% difference in the amount of Nickel will result in a 10ºC difference in the start temperatures of material. If lower or higher start temperatures are desired this

can be accomplished with the use of doping elements such as Chromium. Raytheon uses doped NiTi to produce SMA clamps for military aircraft. The transformation temperatures are well below freezing. The cold joint is stretched to fit over the pipes, and then when heated to ambient temperature it transforms to austenite stage and shrinks to its memorized size. This results in a joint with constant pressure over all operating conditions.

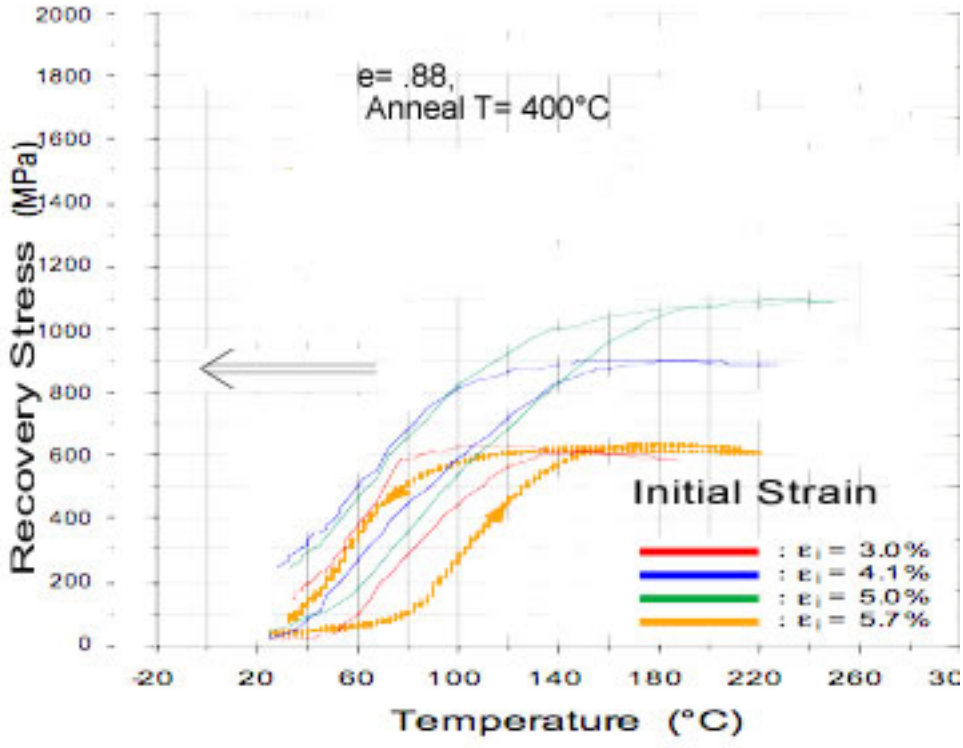

Figure 3-7 Recovery stresses obtainable from NiTi. The lower curves are the generation of recovery stresses from a contrained sample. For deformations of 5% on 1mm diameter wire, streses of up to 1100 MPa are produced. (Demers, 2004)

The cold working is also used to induce the desired properties into the product. It will modify the recovery stresses generated, and the recovery stresses over many cycles. Cold working also results in small changes to the start temperatures, but not of large consequence. (Demers, 2004) The overall temperature transformation range is consistent with a range of approximately 40ºC. (Hodgeson, 1999)

3.3.3 Slotted Steel Saw

One of the designs investigated was the incorporation of slotted saws with shape memory alloys. Slots have been incorporated into saws to reduce vibration, and to relieve stress. Some saw manufacturers incorporate the slots for noise reduction. The location of the slots along the outer periphery allows the steel to expand within this area without the compressive stress generation present in solid saws. The downside of this method is that while the slots result in a saw that overall might have higher natural frequencies, the saw is comprised of cantilevered plates, resultant of these slots, that are less stiff and result in a larger deflection for similar forces. So although the saws can operate at higher speeds, the lower stiffness results in larger kerf loses.

Finite element analysis was used to verify these statements. Overall, the slotted saw showed higher natural frequencies that the solid steel saw under thermal and rotational loads.

The number of slots was determined through simulation. It is preferable for the number of slots to avoid alignment with the modes of vibration. Therefore, 4 slots would decrease the stability of the saw. The 4 slots would align with the modal frequency of interest, the 2 diameter, 0 circumference mode. The 5 slots or 7 slots saws would coincide with the 5 and 7 diameter modes, yet these are not a factor in saw blade stability as these modes have a much higher frequency.

The depth of the slots was also investigated. In most commercial saws the depth of the slots are comparable to the length of the teeth. This is much shorter than the range compressive hoop stresses discussed previously. As stated previously, the hoop stresses are prevalent in the outer 1/5 of the disk. (Dugale, 1965)

3.3.4 Press-fittings

The idea of press fitting bands of SMA was investigated and decided against. This was largely due to difficulties of making sure that the SMA would indeed remain in the saw and not separate. Such a scenario could prove fatal, and without certainty to the inserts remaining in the saw its commercial prospects would be slim and therefore this design was not perused.

3.3.5 General Shape Memory Alloy Design

The general design thought to be most beneficial with the best characteristics was to use a slotted saw as shown in the SMA threaded saw, Figure 3-8. This design is applicable in this situation if SMA inserts are used to bridge the slots as developed in sections 3.3.6 and 3.3.7. The SMA, which will be inducing a tensile stress into the saw throughout operation, will decrease the amplitude of the deflection, while the slots will allow near constant natural frequencies of the stationary saw.

The SMA would either be placed on the saw used a mechanical fastening technique or by sandwiching the steel saw around strips of SMA. Both these techniques would incorporate the use of slots along the outer edge of the saw.

3.3.6 Shape Memory Alloy Threaded Saw

Another design that was simulated was again the slotted saw in which the slots were stitched across by the use of shape memory allows. (Figure 3-8, Figure 3-9) The advantage of this design is that little heat is required in assembly of the saw, only to ‘tie off’ the ends of the SMA string.

The martensite state of SMA is quite deformable, especially in small diameter wire and therefore such a process could be attempted. Also, much research has been put into the

development of SMA composite fabrics, where SMA wire is woven with common composite threads such as carbon fiber and Kevlar. (Schrooten, 2002)

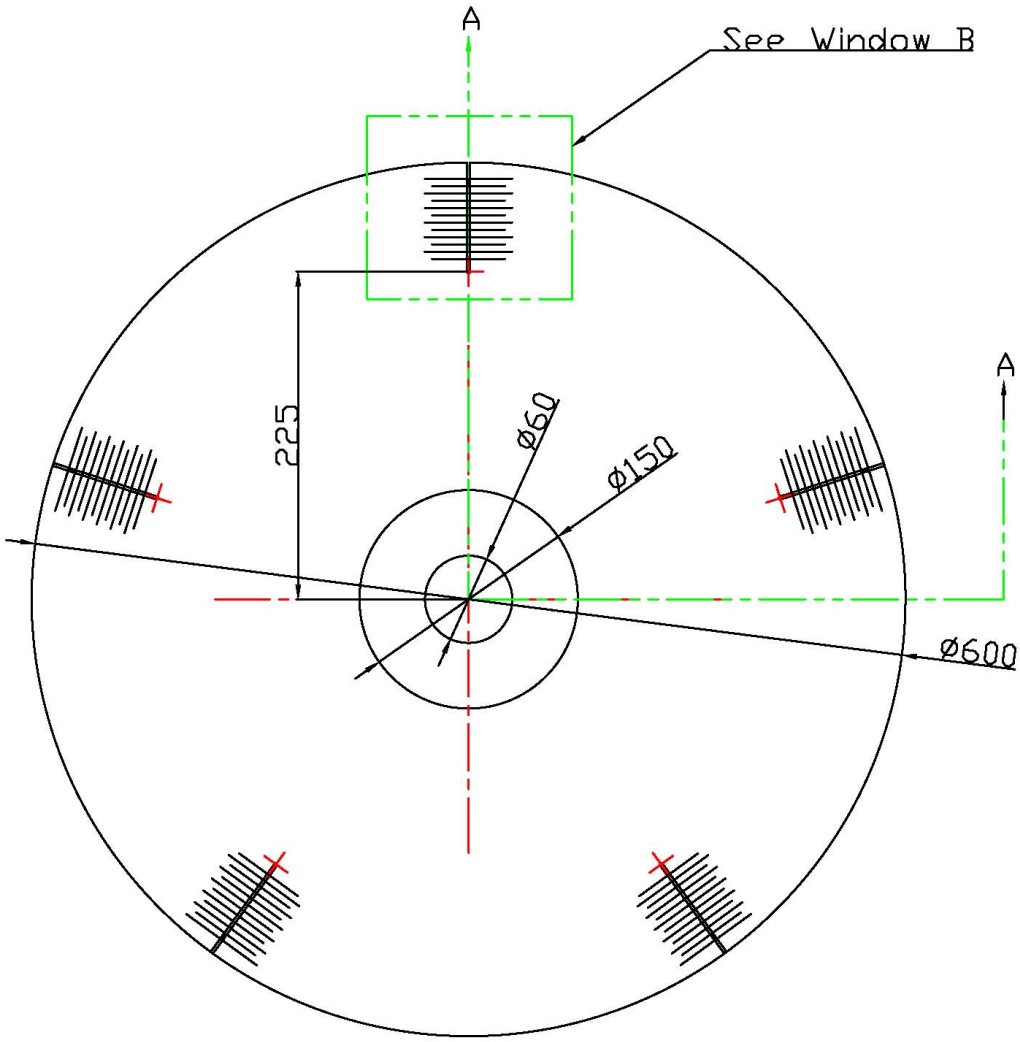

Figure 3-8 Top view of threaded saw.

Although this simple design would take more work for a production capable model, it is an easy method to prove the concept as much of the difficulties of working with SMA are removed. The wire is also easily purchasable from resellers, as there is high demand in research applications and medical devices. The other benefit is that the properties of the SMA are much better established in small wire form as proposed than in large wire form.

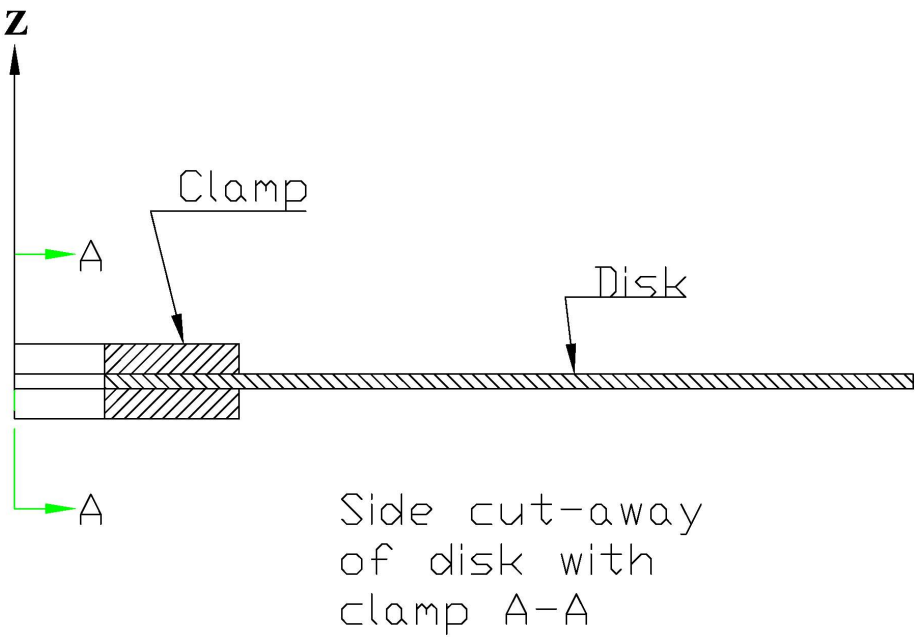

Figure 3-9 Side cut-away of disk.

The wire also benefits from repeatable cold working. The thin wire shows consistent properties and larger constraint forces that would the sheets.

Although the first prototypes will have the SMA protruding from the surface plane of the disk, it will not affect the convection properties of the disk, neither will the drag produce forces significant to this study. These problems will be mitigated through design and manufacturing optimization and prototyping. The purpose of this analysis to simulate a workable model that is capable of production with relatively small design modification.

This differs from previous simulations where the composite saw was an ideal saw that had little possibility of being put into production. This saw design is quite suited to iterative design and building.

The threading consisted of 8 rows of holes on either side of the slot, starting at 5mm from the edge of the slot, the rows consisted of holes every 10 mm from the base of the slot to

the edge of the saw as seen in Figure 3-10. The holes on successive row were staggered 5 mm from the previous row. Each hole was 1mm in diameter with a 1mm SMA wire running to the hole opposite the slot. (Figure 3-11)

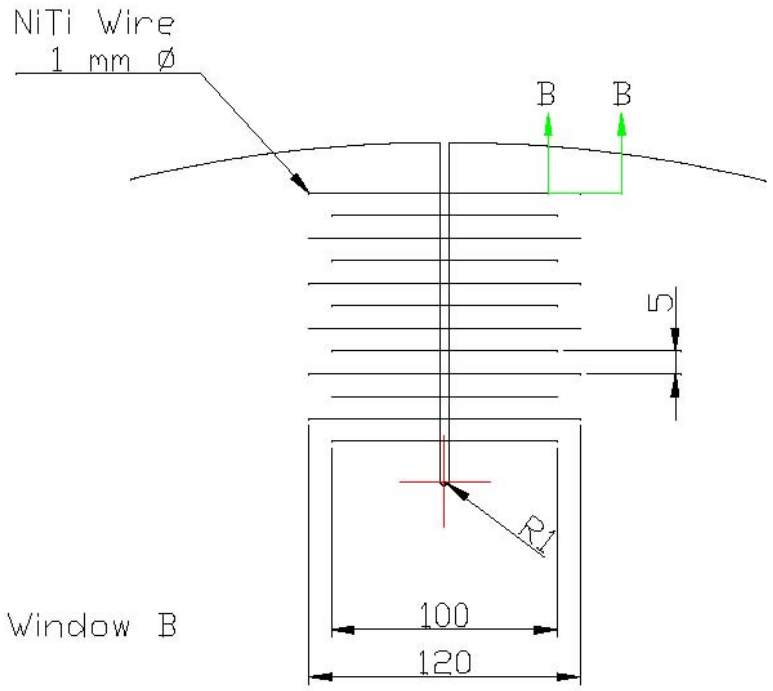

Figure 3-10 Threaded disk close up of window B from Figure 3-8.

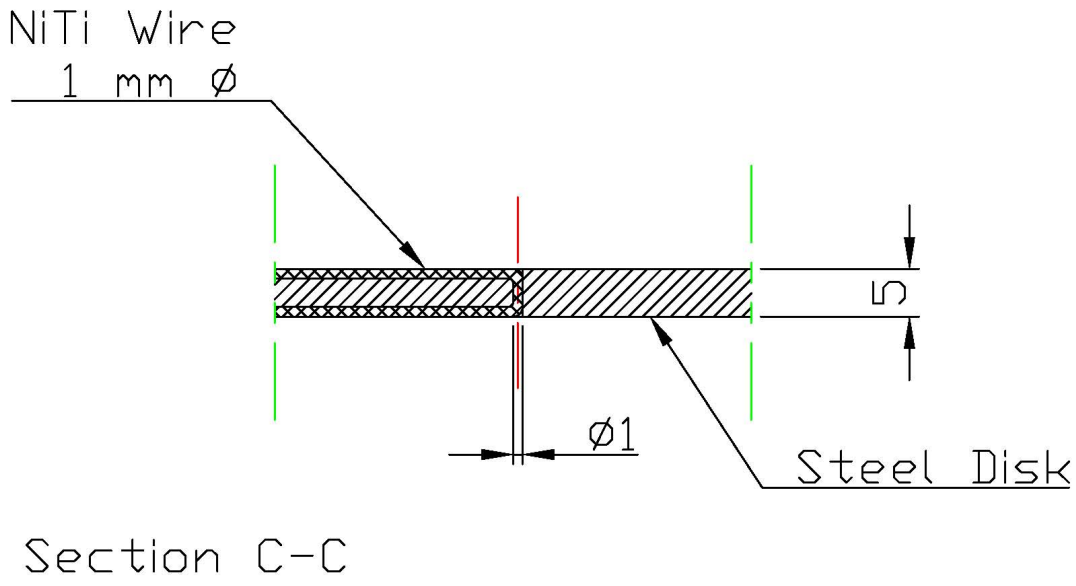

Figure 3-11 Enlarged cut-away of threaded section.

3.3.7 Composite Shape Memory Alloy Inserts

There are two design possibilities to this design, first involves mechanically fastening the strips of SMA to the saw. The other design consists of sandwiching the strips of SMA within two steel halves of the disk. These strips would fit into hollowed out areas of the saw. The ends of the SMA strips would be retained in the steel by obstruction. Also pegs in the steel would help retain the strips., as seen in Figure 3-12. After this the two halves of the steel saw would be placed together. To keep the two halves together, spot welding and fastener are used. Fasteners are less of a problem in this situation as they are not being acted upon by the SMA strips and therefore need not be as robust. They are primarily a safety mechanism in case of failure of the welds. The use of a saw involving several layers is not a radical idea as there have been laminated steel saws used as prototypes. (Szymani, 1984)

Another benefit of this design is that the localized heating of the saw by spot welding would not induce the shape memory effect of the SMA strips. Therefore while joining the

saw would not be stressed by the SMA strips and the welds would be acceptable. The use of pressure can be used to compensate for a lower welding temperature. (Smallman, 1999) The possibility of welding to stainless steel also exists. (Wang, 1997)

Tests were performed with ANSYS to see where the stability of the saw is greatly affected by the depth of the slot. In this case, the heat distribution of the saw is said to be similar to the heat distribution of a non-slotted saw. The small increase in surface area around the slots is not enough to change the temperature profile. Secondly, these slots are often clogged in the cutting action, limiting its ability to dissipate heat.

The optimum depth of the slot allowed the use strips of SMA of sufficient width to be used. One of the constraints of the use of the SMA was the large forces generated and the need to constrain the material. As such, the joining area is much wider than the area in which the SMA is acting as a tensioning device.

The inserts consisted of 1 mm thick samples 5 mm wide at the neck. The neck portion was deformed to produce 200 MPa of stress when heated while constrained. The ends of the sample are 10 mm wide.

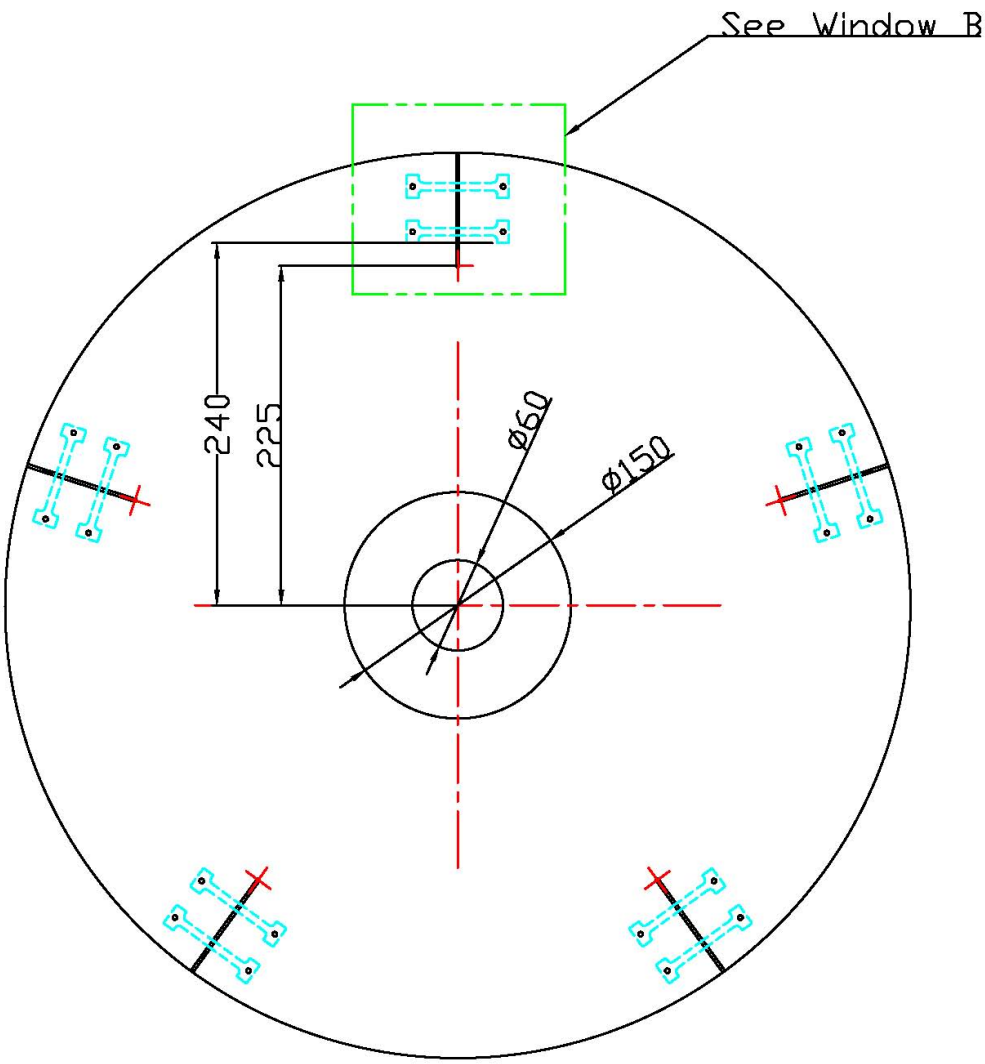

Figure 3-12 Design of SMA insert saw.

For overall results of the either testing method the design of the saw has been simplified to that of the riveted SMA strips. It is assumed that the two halves of the sandwiched saw were joined in such a manner that the saw acts a single piece with SMA acting in distinct points on the saw. The same is said with the riveted saw with the SMA acting upon the rivets that in turn act upon the steel of the saw.

The SMA inserts consisted of a 1 mm thick SMA plate sandwiched between two halves of the steel saw. The plate extended 33 mm to either side of the slot and was the depth of the slot as demonstrated in Figure 3-13.

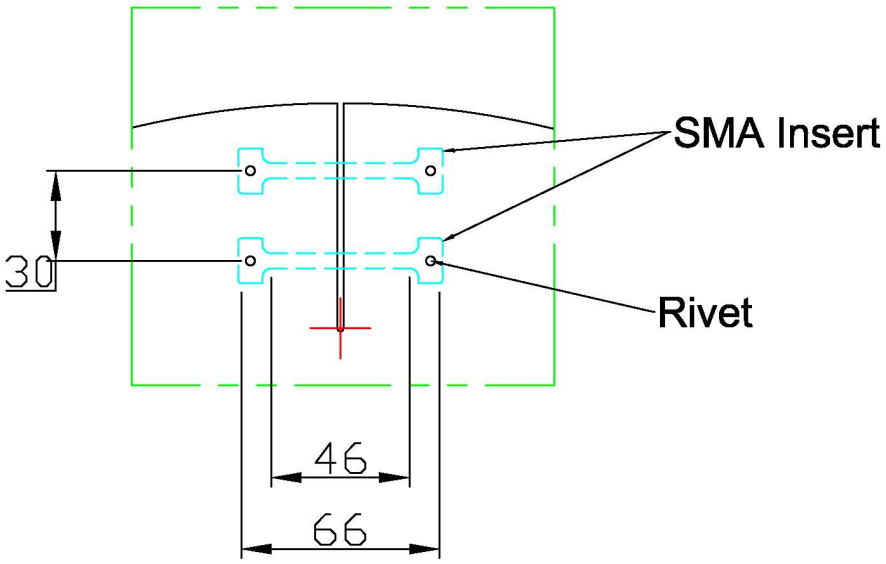

Figure 3-13 Close up window of SMA inserts.

3.3.8 Shape Memory Alloy Assumptions for Design

The strips of the SMA must not fail within the saw, nor should they cause failure to the saw. Therefore, for the saw incorporating mechanical fasters, common machine design outlines are used in the calculation of the strength of the SMA. The SMA wires would produce a maximum of 200 MPa of recovery stress. They would induce a maximum of 400 MPa of stress into the saw, 21% of the yield strength of AISI L6 tool steel (1900 MPa) commonly used in saw blades. In these cases, the SMA limited from having the maximum values for recovery stress possible by the machine design limits. The design requirements of the saw are such that the SMA is trained with recovery stresses well below the maximum attainable, and below the design limitations imposed.

For the insert design, the SMA strips will be acting on pegs and constraints in the hollowing out of the disks. These constraints will have properties of the saw steel and will fail as though a homogeneous material. Welding points are such that the welds do not occur in areas where the SMA and steel would have contact stresses.

The properties for the steel disk are the same as those used in previous designs.

3.4 Design Selection

Different designs were put forward and studied and are described in section 3.3. The criterion for the design is largely based on the ability of the design to be built and the improvement in operation. Economic feasibility, manufacturing complexity, and durability are important to the design process but not a requirement. Table 3.4 outlines the criteria used to judge the different designs. From this exercise with the Pugh matrix it was possible to determine that based on the criteria use and the estimates of the value of each criteria as it compares to the standard it was possible to see that the threaded SMA saw seems to be the best choice for further development. Further analysis will be needed to confirm this.

The criteria used in the Pugh matrix were judged on a scale of 1 to 3. A greater emphasis was placed upon improvement in operation, including over a range of operation. Therefore greater weight was given to kerf, stability and adaptability. Manufacturability (Assembly and machining) and safety (Disk failure and dislodged objects) where not weighed as heavily as these were given multiple criterion, and were better adapted to a pass-fail selection. The designs do meet safety and manufacturability as explained in sections 3.2.2 and 3.2.3. Cost and material procurement were weighed as standard with a weight of 1.0.

The material to be used would be NiTi as before. This material has been the most extensively studied of all the SMA. It has also seen use outside of the laboratory setting, from aerospace, temperature controls, robotics, and in medical implants. As NiTi is often used for medical implants, there are several manufacturers and resellers, allowing the ready acquisition of the material, versus the additional requirements of founding that would be incurred with the use of a different type of shape memory alloy.

Table 3.4 Pugh's matrix comparing different designs.

Concept / Criteria	Standard: Pretensioned Saw	Slotted Saw	Threaded SMA Saw	Saw with SMA Inserts	Criteria Weight
Cost	3	3	2	1	1
Manufacturability (Assembly)	3	3	2	1	0.5
Manufacturability (Machining)	3	3	2	1	0.5
Safety (Disk Failure)	2	3	2	2	0.5
Safety (Dislodged Object)	3	3	2	1	0.5
Material Procurement	3	3	2	1	1
Stability	2	1	3	3	1.5
Kerf	2	1	3	3	1.5
Adaptability	1	2	3	3	1.5
Total	22	22	21	16	
Weighed Total	19	18	21.5	18	

The proposed designs in this thesis are based on designs that can be accomplished with available machining and manufacturing processes.

3.5 Summary

Previous designs of a disk with SMA showed the ability to increase stability in the disk under rotation and subject to thermal forces. The previous design was advanced to one that can be manufactured while meeting safety, productivity and economic concerns through common design methodology.

The safety of a design is always of concern. In the sawmill setting the hazard posed by circular saws have been recognized, and several methods of mitigation have been implemented, including guarding, automation, and creation of hazards zones where the placement of operators is avoided.

The manufacturability of the saw is addressed through conventional fabrication techniques such as fasteners and mechanical interfaces. Machining techniques currently used in the production of circular saws, such as grinding and laser or water cutters, are applicable to the fabrication of the proposed design. The production of NiTi is established and a standardized process would produce the SMA inserts in an economical fashion.

Proposed techniques of integrating the SMA into the saw include threading, use of mechanical fasteners, composite material of NiTi wire and filament within epoxy, and integration of SMA into the saw through sandwiching between two plates to form a disk. These designs were evaluated using quantitative design analysis, and it was found that the threaded saw was the best of the proposed designs.

4 Analysis Parameters and Assumptions

For the analysis of the proposed design, the properties of the materials used and any assumptions used are explained. The models for the simulating the designs are refined through comparisons to established software and prior literature. The modeling of the designs for finite element analysis is explained for the proposed designs. The methods used to obtain measurements for disk deflection, stresses, natural frequencies, and critical speed are described.

4.1 Material Properties

4.1.1 Shape Memory Alloys

The NiTi used in the analysis is 50.4 % titanium, remainder nickel. The material was cold worked to $\varepsilon = .81$ and annealed at 400ºC. With these attributes; the alloy has the following properties. (Table 3.1, Table 3.2)

Table 4.1 NiTi properties.

Properties of NiTi	Martensite	Austenite	
Young's Modulus of Elasticity (E)	40	80	GPa
Poissons Ratio (μ)	0.3	0.3	
Density (ρ)	6450	6450	kg/m^3

Table 4.2 NiTi Phase change temperature.

Phase Change Temperature	
Austenite Start	Austenite Stop
40ºC	80ºC

4.1.2 Steel

The properties of the L6 tool steel used in circular saws and in the simulations are provided in Table 4.3.

Table 4.3 Steel properties.

Properties of Steel	
Young's Modulus of Elasticity (E)	2.00E+02 GPa
Poissons Ratio (mu)	0.3
Thermal Coeffcial of Expansion (alpha)	1.06E-05 m/m
Density (rho)	7450 kg/m^3

4.2 Finite Element Analysis

For all of the following analysis the finite element analysis program ANSYS versions 7.0 and 10 were used.

4.2.1 Disk Dimensions

Due to the thin dimensions of the disk, shell elements were used to simulate the disk. The clamp was incorporated into the saw and modeled at thicker shell elements.

The dimensions of the disk are as outlined in Table 4.4., where **a, b, H, d,** are the dimensional version of the non-dimensional measurements shown in Figure 2-1, and Figure 2-2.

Table 4.4 Disk dimensions.

a	0.075	m
b	0.300	m
H	0.0025 - .0015	m
d	8	

4.2.2 Meshing and Refinement

Simple design as shown in the Figure 2-1 was used to establish a solid model of the saw. The solid model was then meshed using ANSYS meshing tool, Figure 4-1. Triangular elements were used to model the saw. The meshed saw was subjected to stresses including rotation and thermal and analyzed. The model was refined in areas of high stress using the mesh refinement tool in ANSYS, Figure 4-2. As a result of the wire links and slot meshes were highest around the slot: see Figure 4-3 and Figure 4-4. The analysis was iterated until changes in stresses were less than 1 %. The models displayed incorporate the mesh refinement used in the results. (Zienkiewicz, 2000)

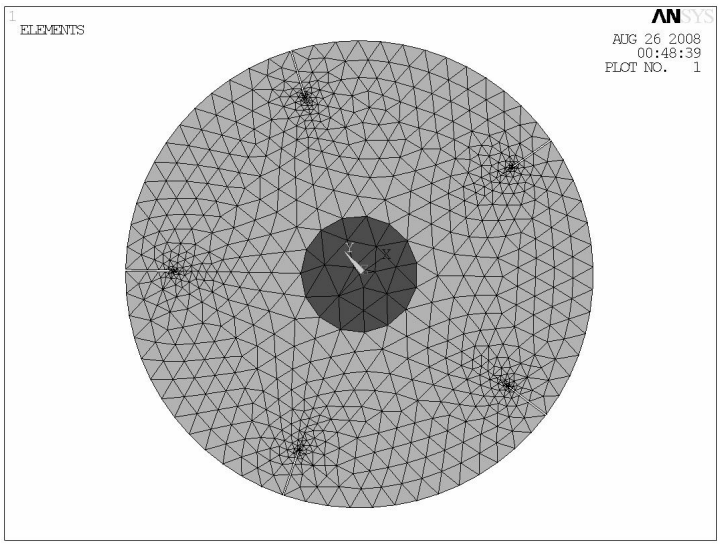

Figure 4-1 Disk meshing.

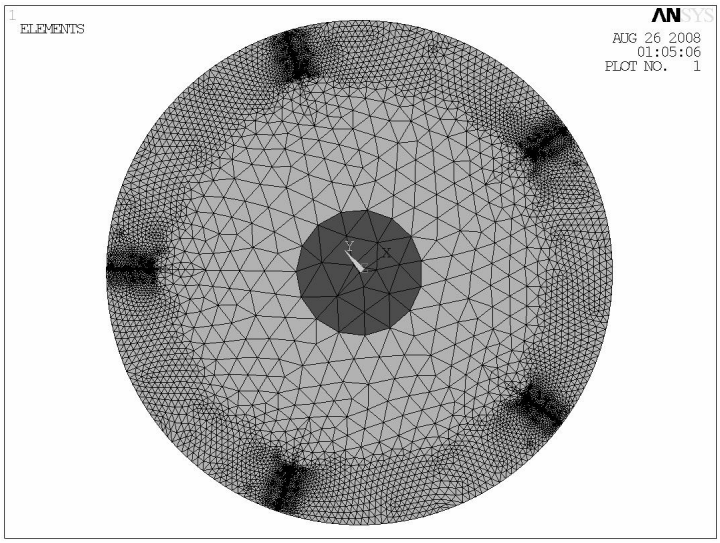

Figure 4-2 Disk mesh refinement.

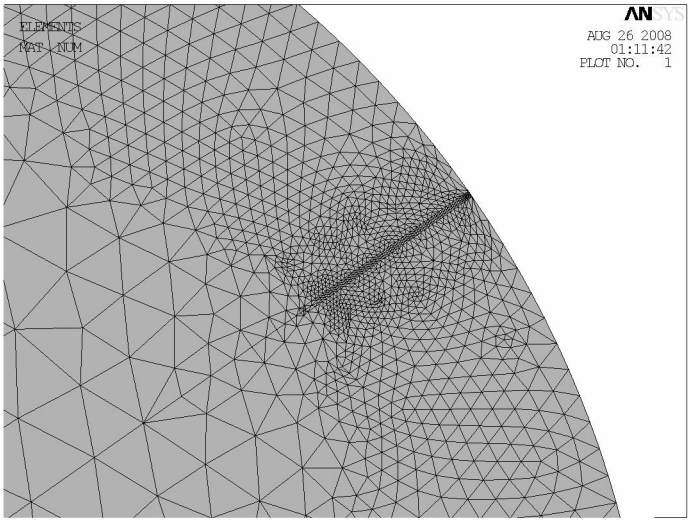

Figure 4-3 Mesh refinement: close-up of slot.

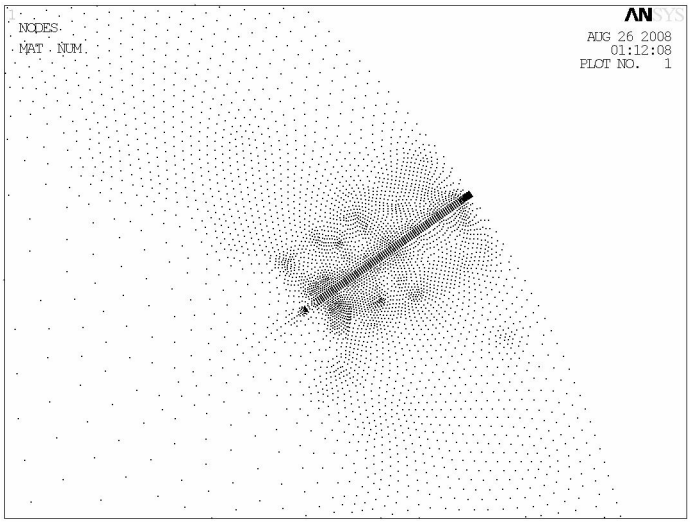

Figure 4-4 Node placement: close-up of slot.

For elements, the model used shell plate elements. For the SMA inserts these were modeled as mass-less links for the shape memory effect. The mass and stiffness properties of the SMA inserts was added to the disk shell element as a layer.

4.2.3 Boundary Conditions

The boundary conditions of the model were similar to those used by Mote in his analysis of the spinning disks. (Mote, 1967) The edge of the disk at $\mathbf{r_b}$ was unconstrained. At $\mathbf{r_a}$ the disk is continuous with the clamp and inner disk. The disk is constrained at $\mathbf{r_a}$ in every degree of freedom except the **r** direction. No rotation is allowed at $\mathbf{r_a}$. At the center of the disk, the disk is fully constrained.

4.2.4 Application of Forces and Temperatures

The temperatures and rotations applied were similar to those encountered by saw blades. The temperatures applied to the saw at $\mathbf{r_b}$ were from 50ºC to 150ºC. For rotation speed, 100, 200, and 300 radians per second were applied. These approximate 1000, 2000, and 3000 rpm, which are typical non super-critical operating speeds. (Quelch, 1964)

The distribution of temperatures was calculated using Maple. The temperature profile as shown above was then used in all the analysis programs. The temperature profile was dependant on temperature at $\mathbf{r_b}$, disk thickness, and rotation speed. With the addition of SMA, or slots to the saw, the assumption was made that these were of negligible effect to the temperature profile of the saw.

After application of the temperature and rotation, a stress analysis was performed. The results of the stress analysis were inputted into the modal analysis. For ANSYS the Block Lanczos analysis method was used. (ANSYS, 2005)

4.2.5 Deflections

To measure the possible width of the kerf, the amount of deflection of the edge of the saw was investigated. For the solid steel saw and the ideal composite saw, this was done by finding the defection of the edge of the saw when presented to a point load as seen in Figure 4-5. The force applied was 100 N.

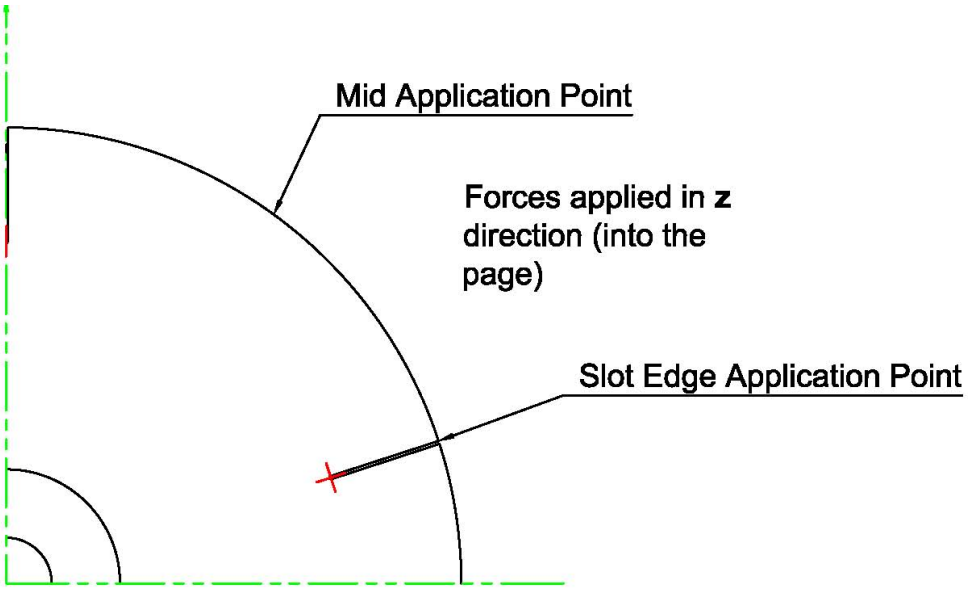

Figure 4-5 Deflection simulation applied point.

4.3 Tensioning

To simulate the effect of pretensioning, a temperature profile was used to simulate the deformation and stresses induced by the rolling. This temperature profile was added to the temperature profile present due to heating (Figure 4-6). The tensioning acts at .78 $\mathbf{r_b}$. This is the same method as applied in Kuratani. (Kuritani, 2000)

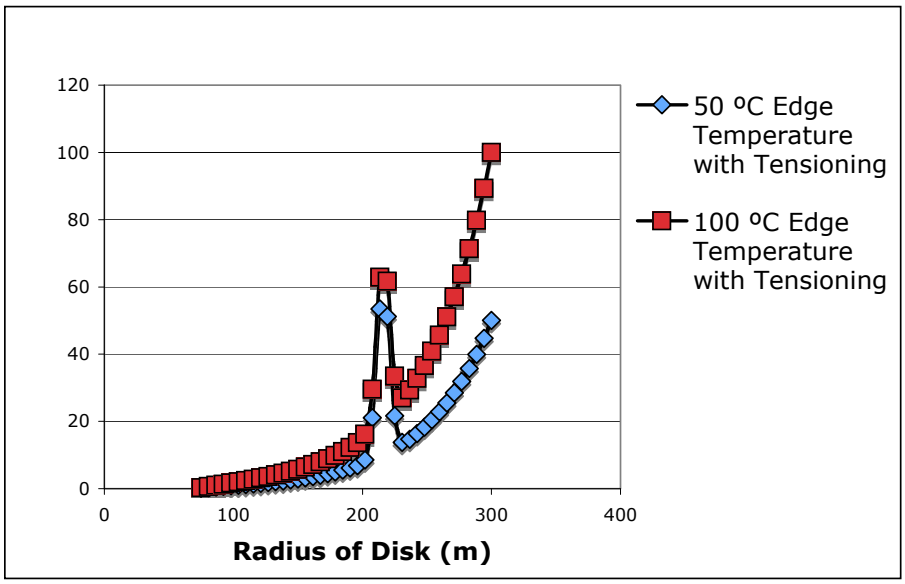

Figure 4-6 Tensioning temperature profile.

4.3.1 Simulating the Shape Memory Effect

To simulate the shape memory effect, the shape memory alloy was modeled to have a negative coefficient of thermal expansion in the direction of the shape memory recovery. Between $\mathbf{T_{As}}$ and $\mathbf{T_{Af}}$ the SMA is modeled to respond in a linear fashion. The rate of strain produced between these two points was linear. To produce a recovery stress of 200 MPa , a coefficient of thermal expansion of -10.6 $\frac{\mu m}{m°C}$ relative to $\mathbf{T_{As}}$ is required. This negative coefficient of thermal expansion is applied between $\mathbf{T_{As}}$ and $\mathbf{T_{Af}}$. Below $\mathbf{T_{As}}$ the the martensite phase of the material has a thermal coefficient of +10.6 $\frac{\mu m}{m°C}$ relative to 0

°C is used while for it coefficient of thermal expansion while above $\mathbf{T_{Af}}$, 18 $\frac{\mu m}{m°C}$ relative to $\mathbf{T_{Af}}$ is used. To properly use these properties in the FEA, the values were all set relative to 0 °C. The resulting function for the coefficient of thermal expansion for the analysis is shown in Figure 4-7, along with the linearized version used in the ANSYS program.

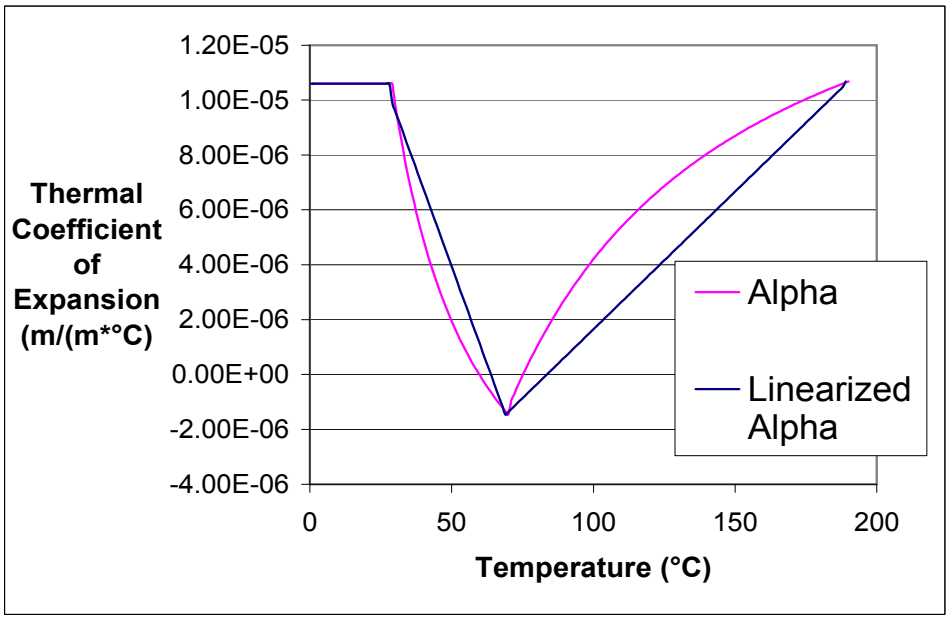

Figure 4-7 Value of coefficient of thermal expansion for SMA.

4.3.2 CSAW Analysis Tool

CSAW is a computer simulation program designed to compare tensioning techniques on circular saw blades. This program has been accepted by the forest industry and has been validated against industrial saws. G. Schajer, who has done extensive research into the problem of saw blade stability, developed the program in the 1989. It uses the Rayleigh-Ritz-Galerkin method to obtain the solution of the eigenvalue problem. The stress is calculated as outlined in chapter 2. (Schajer, 1995)

The program requires the user to provide the material properties, the physical dimensions, the operating speeds, and any applied loads including temperature. The program will calculate the critical speeds of the various modes and also the modal frequency. However, the program can only simulate the behavior of existing saws and cannot be used to simulate saws with tapered profiles or dissimilar materials such as SMA inserts.

The temperature profiles of the disk were obtained by the method described previously in section 2.1 using MAPLE. The CSAW simulations will be used as a basis to refine and validate the finite element model.

4.3.3 Modal Analysis and Critical Speed by Finite Element Method

The modal frequencies for varying rotation speeds were obtained for the temperature profiles imposed. The modal frequencies were given relative to the frame of reference of the spinning saw. The critical speed of the saw was obtained by changing the frame of reference to a stationary observer. This allowed the tracking of the modal frequencies until they reached close to zero for the rotating observer or less than zero for the stationary observer. At this point, the critical speed of the saw was obtained through interpolation.

4.3.4 Ideal Composite Saw

The ideal composite saw was comprised of a steel saw with SMA bands perfectly affixed to the outer edge of the saw. For the area of the saw between .8 $\mathbf{r_b}$ and $\mathbf{r_{b,}}$, the saw consisted of a laminate of SMA-Steel-SMA with the SMA bands 20 % of the thickness of the saw and the steel 60% of the thickness. The SMA bands were deformed 2% prior to being attached in such a manner as to cause them to contract in the hoop direction when warmed.

4.3.5 Slotted Steel Saw

Slotted steel saw was simulated for different number of slots from 4 slots to 9 slots. The size of the slots was kept constant. The width of the slot was large enough that sides of the slot would not touch due to thermal expansion for a 300 mm radius disk with edge temperature 150ºC relative to ambient and a rotational velocity of 300 radians per second. The same temperature profile as applied for the composite and steel saws were applied.

To simulate the disk the following assumptions were made:

i. The wire will not cut through the disk The use of hardened L6 tool steel in the saw design is hard enough to prevent the NiTi from cutting through the steel, as would be seen if the disk was made of aluminum or another alloy with a yield strength less than that of the L6 tool steel used in the design.

ii. The holes through which the SMA is threaded will not fail. The holes will contain the forces produced by the SMA but will not deform permanently.

iii. The SMA will not be cut by the edges of the holes. These holes are shaped in such a manner to prevent the failure of the device or the SMA.

4.3.6 Composite Saw with Inserts

To simulate the inserts, a similar FEA model to the threaded saw is used. As rivets or mechanical fasteners would retain the inserts, the effect of the shape memory effect would act upon a discrete points on the steel structure similar to the threaded saw pattern as the threaded saw. The major difference between the use of wire and the use of inserts is that the inserts shape memory effect would be weaker than that of the wires due to greater difficulty producing SMA strips that shows as great a memory effect as SMA wire.

The model used is similar to the threaded saw, although the slot is now spanned by SMA material 20% the thickness of the saw, and the number of threads has been decreased by half.

4.4 Summary

To achieve a reliable finite element model for simulation of the design several validation techniques and assumptions were used. The finite element model was refined through comparisons to a commercial saw simulation program, CSAW.

The simulation of the NiTi necessitates the use of temperature dependant properties. For the elasticity, the material's properties are proportional to the composition of austenite and martensite within the material. For the shape memory effect, the material is modeled as having a negative coefficient of thermal expansion. The use of tensioning in the saw is modeled through the application of a thermal stress similar to the actual resultant stresses in a pre-tensioned disk.

5 Results and Discussion

The finite element model developed to simulate a steel saw is compared to CSAW, an industrial saw simulator. The finite element model for the proposed designs are simulated to obtain deflection, stress and frequency information. The model is also compared to a current tensioning technique, pretensioning, with similar results. Overall, the results of the model's simulation are compared to current saws in practice and the previous design.

5.1 CSAW Validation

The two methods, FEA and CSAW, were compared with the goal of finding agreement between the two software methods. For low speeds and low temperature stressing, both the FEM and the CSAW produced similar results. At higher edge temperatures, and greater speeds of rotation, at conditions that are near critical and result in small natural frequencies values, it was found that there were larger variations between the results of the two programs.

The boundary conditions are the largest contributor to this discrepancy. When the boundary conditions as found in Mote (1967) are applied, where the disk is bound at the center axis and the saw clamp area is modeled as being part of the saw, although thicker, the resultant natural frequencies are found to be lower than those produced by CSAW. These differences are found to be greater on the thinner saws. On the 3.0 mm thick saw, the FEA program using the above clamping conditions would calculate that the mode of frequency would not be present, when it was present with the CSAW application.

With the modified clamp boundary conditions, the FEA was able to produce the same modes of vibration that CSAW had produced, within the error of CSAW. The frequencies were in most cases within 1 Hz of each other. (Figure 5-1, Figure 5-2) Where the membrane stiffness is of greater significance and the speeds were near critical the difference is more pronounced but still within 3-5 Hz. (Figure 5-3) This is also explained

by the use of the Rayleigh-Ritz-Galerkin method that produces results that are higher than the true value. (Schajer, 1995)

Overall, the FEA model did produce similar results and did trend well with the CSAW program. Better agreeability would be possible, but only at a significant cost to computing resources and speed of the simulations. As most industry saws operate at less than 80% critical speed, the need for the greater accuracy at critical speed is less important.

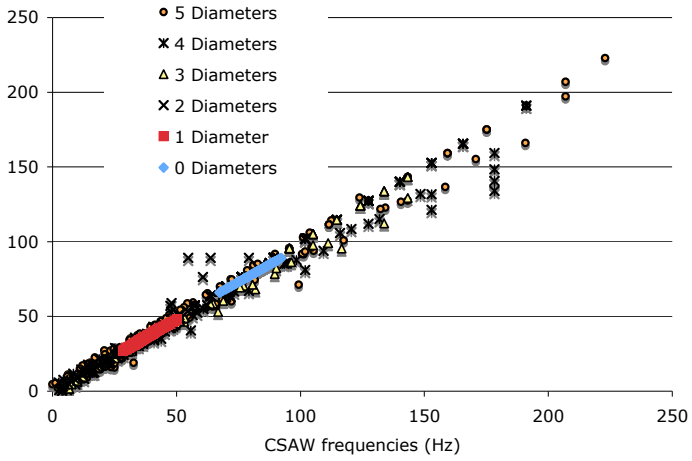

Figure 5-1 Comparison of frequencies obtained by CSAW and ANSYS for 3mm steel saw.

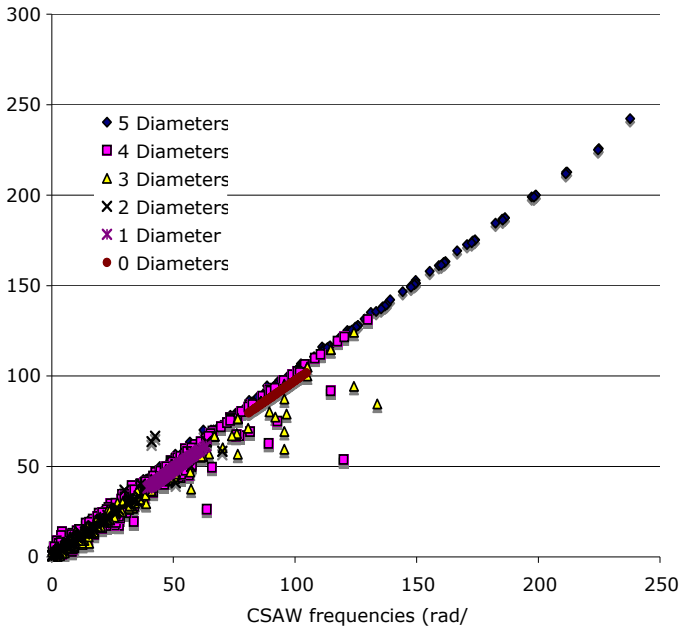

Figure 5-2 Comparison of frequencies obtained by CSAW and ANSYS for 4mm steel saw.

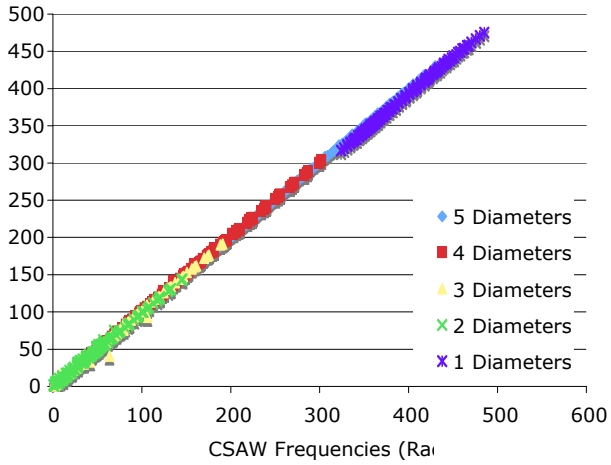

Figure 5-3 Comparison of frequencies obtained by CSAW and ANSYS for 5 mm steel saw.

5.2 Tensioning

The most common method of stiffening saws; the tensioning produces steels saws that are more stable than untentioned saws when used in normal operating conditions. When

the tensioning technique is applied to the ideal composite saw, the stability of the saw is similar to that of the slotted saw.

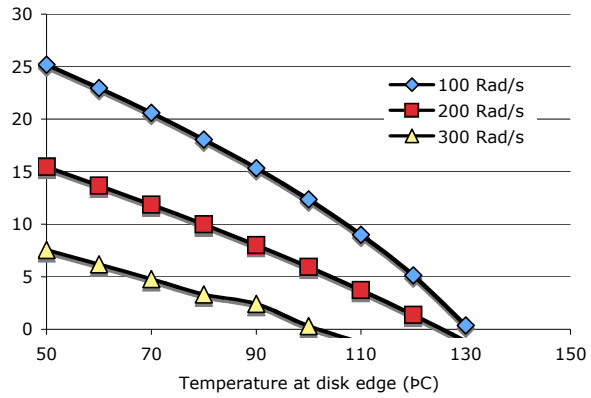

Figure 5-4 5 mm thick steel saw blade with tensioning (2 diameters, 0 circles).

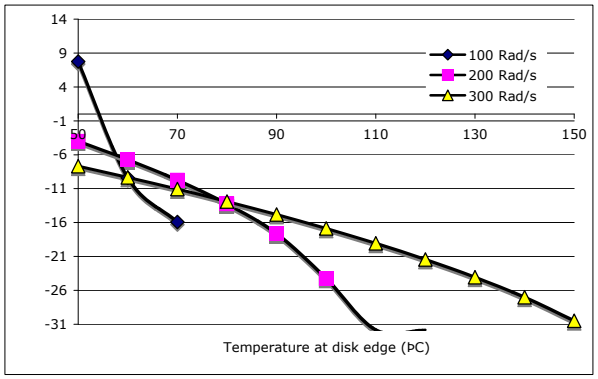

Figure 5-5 3 mm thick steel saw blade with tensioning (2 diameters, 0 circles).

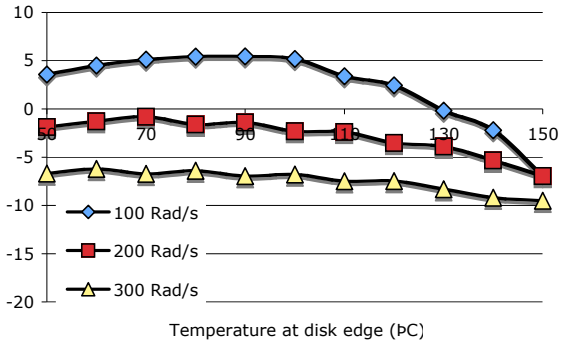

Figure 5-6 3 mm thick ideal composite saw blade with tensioning (2 diameters, 0 circles).

5.3 Deflections

When comparing the deflection of the edge of the saw at $\mathbf{r_b}$, the deflections are similar for the forces applied between the two slots on the slotted saw and for the ideal composite saw at the edge. (Table 5.1, Table 5.3) As the number of slots increase, so does the amount of deflection of the saw. For the high number of slots, the area between the slots will bend in a similar fashion as a plate clamped along a line between the depths of two neighboring slots in addition to deflections of the saw as a whole.

For the edge of the slots, the deflections are much larger than those encountered in between the two slots as could be predicted. With the threaded saw, the deflections encountered were less than the slotted saw as a result of the threads providing increased stiffness to the saw. (Table 5.2)

Table 5.1 Deflection of ideal composite saw.

Disk thickness (m)	Deflection of edge (m)
0.005	6.58E-04
0.004	1.28E-03
0.003	3.04E-03

Table 5.2 Deflection of threaded saw.

Disk thickness (m)	Number of slots	Deflection at corner (m)	Deflection between slots (m)
0.003	7	3.24E-03	2.96E-03
0.003	8	3.28E-03	3.02E-03
0.003	9	3.32E-03	3.06E-03
0.004	7	1.37E-03	1.25E-03
0.004	8	1.39E-03	1.28E-03
0.004	9	1.41E-03	1.30E-03
0.005	7	7.07E-04	6.45E-04
0.005	8	7.16E-04	6.56E-04
0.005	9	7.24E-04	6.65E-04

Table 5.3 Deflection of slotted saw.

Thickness (m)	Number of slots	Deflection at corner (m)	Deflection between slots (m)
0.0030	4	3.15E-003	2.87E-003
0.0030	5	3.18E-003	2.92E-003
0.0030	6	3.21E-003	2.95E-003
0.0030	7	3.25E-003	2.99E-003
0.0030	8	3.28E-003	3.03E-003
0.0030	9	3.31E-003	3.08E-003
0.0030	10	3.34E-003	3.12E-003
0.0035	4	1.98E-003	1.81E-003
0.0035	5	2.01E-003	1.84E-003
0.0035	6	2.03E-003	1.86E-003
0.0035	7	2.05E-003	1.89E-003
0.0035	8	2.07E-003	1.91E-003
0.0035	9	2.09E-003	1.94E-003
0.0035	10	2.11E-003	1.97E-003
0.0040	4	1.33E-003	1.22E-003
0.0040	5	1.35E-003	1.23E-003
0.0040	6	1.36E-003	1.25E-003
0.0040	7	1.37E-003	1.27E-003
0.0040	8	1.39E-003	1.28E-003
0.0040	9	1.40E-003	1.30E-003
0.0040	10	1.41E-003	1.32E-003
0.0045	4	9.37E-004	8.54E-004
0.0045	5	9.47E-004	8.67E-004
0.0045	6	9.57E-004	8.78E-004
0.0045	7	9.67E-004	8.90E-004
0.0045	8	9.77E-004	9.02E-004
0.0045	9	9.86E-004	9.15E-004
0.0045	10	9.95E-004	9.27E-004
0.0050	4	6.84E-004	6.24E-004
0.0050	5	6.92E-004	6.32E-004
0.0050	6	6.99E-004	6.41E-004
0.0050	7	7.06E-004	6.49E-004
0.0050	8	7.13E-004	6.58E-004
0.0050	9	7.20E-004	6.67E-004
0.0050	10	7.27E-004	6.77E-004

5.4 Modal Analysis

5.4.1 Ideal Composite Saw

When compared to the steel saw, the ideal composite provides for a stiffer saw under heated operating conditions. As seen in Figure 5-7, the saw delays the onset of instability by a temperature range equivalent to the range between $\mathbf{T_{As}}$ and $\mathbf{T_{Af}}$.

As for thickness, at lower speeds and edge temperatures, the ideal composite saw provides for significant decreases in saw thickness. The thickness of the unguided, untensioned saw results in a saw that is equivalent in thickness to a tensioned saw, as can be seen in Table 5.4. This application of SMA also results in a saw that can operate with a higher fundamental frequency when compared to a similar steel saw as seen in Table 5.5.

Table 5.4 Decrease possible in thickness for ideal saw.

Angular Velocity (rad/s)	Fundamental Frequency (rad/s)	Composite disk thickness (mm)	Reduction in disk thickness %
100	77.7	3.55	29.00%
200	32.2	3.72	25.60%
300	21.5	4.41	11.80%

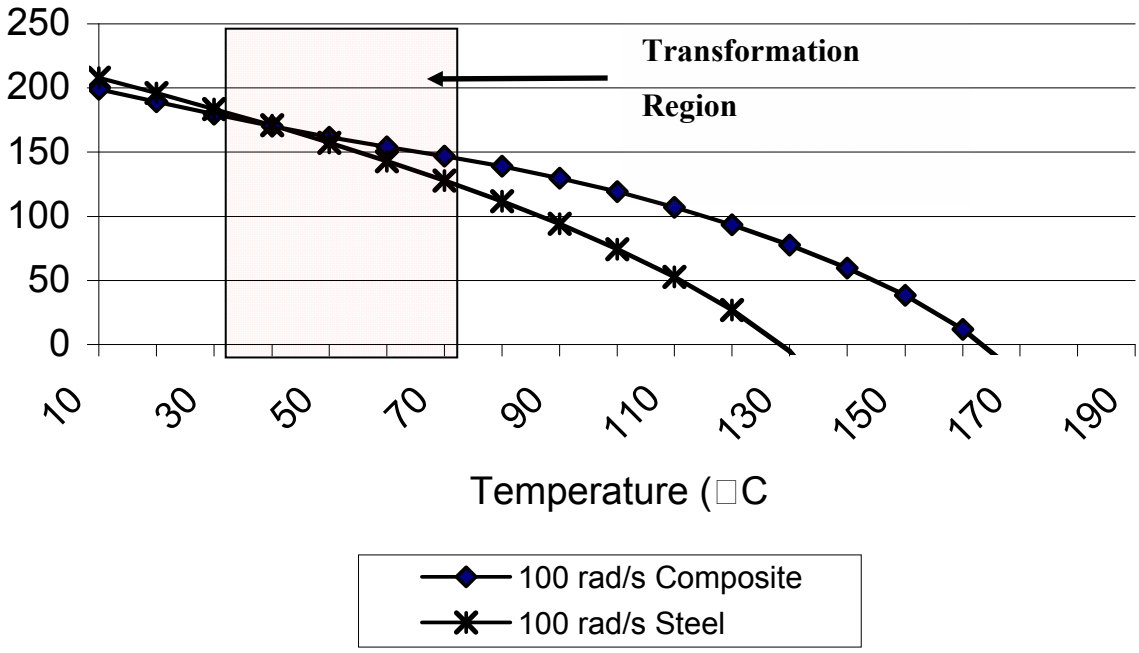

Figure 5-7 Fundamental Frequency of Disk with Angular Velocity of 100 rad/s.

Table 5.5 Improvement of fundamental frequency by the ideal composite saw compared to the steel saw.

	Frequency (rad/s)		
Velocity (rad/s)	Steel Disk	Ideal Composite Disk	Improvement %
100	74.52	119.09	59.81%
150	52.77	89.37	69.36%
200	33.34	63.73	91.17%
240	18.87	44.96	138.27%
300	-1.49	12.36	n/a

5.4.2 Slotted Steel Saw

The slots in the steel saw provide significant stress relief. As a result of the slots the saw is essentially unaffected by the heating. Also of note, due to the slots in the saw, the natural frequencies of the saw are closer to that of a saw of smaller diameter.

A drawback to the slotted saw is that the kerf has the possibility to be much larger. Although the deflections of the slotted saw are comparable to the other saw designs

investigated, the tips of the saw near the slots can deflect in opposite directions, resulting in a kerf that is twice the deflection recorded. Also significant is that such displacement of the saw teeth could lead to the saw binding, and possible failure.

For the slotted saws that have slots that coincide with the nodal diameters (i.e. 4,6,8,9 slotted saws), the saw's periphery will cup between slots. So although a section between the nodal diameters, and slots, is displacing in the positive **z** direction, the edge of the slots will have displaced in the negative **z** direction relative to the plane. Those areas on the other sides of the nodal diameters will be moving in the opposite direction. This results in large changes in displacement between subsequent teeth. As stated earlier, such displacements could result in the binding of the saw, and produces difficulties in attempting to use guides near $\mathbf{r_b}$.

5.4.3 Threaded Composite Saw

The threaded composite saw performed better than the steel saw. Whereas for the slotted saw, slight improvement in stability was seen with increasing number of slots, with the threaded saw this increase in stability was much more pronounced within the increase in the number of slots and where plate stiffness is less of a factor. (Figure 5-8, Figure 5-9) This increase in stability occurs as a result of the use of SMA in the saw. Secondly the SMA was able to become stable at a temperature higher than the onset of instability as seen in Figure 5-10. The higher number of slots provided for a more stable saw. For the 5 slotted saw, it is seen that its critical speed is lower than that of the saws with 7, 8, and 9 slots. (Figure 5-10) The larger presence of SMA in those saws with a greater number of slots contributed to this increase in stability.

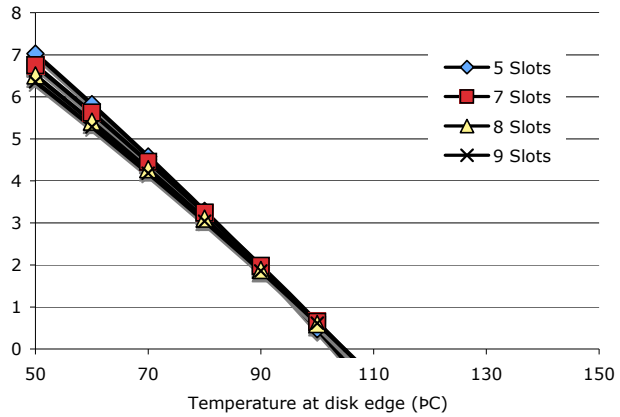

Figure 5-8 Modal Frequency (2 dia., 0 cir.) versus number of slots for threaded saws 5mm thick at 300 rad/s.

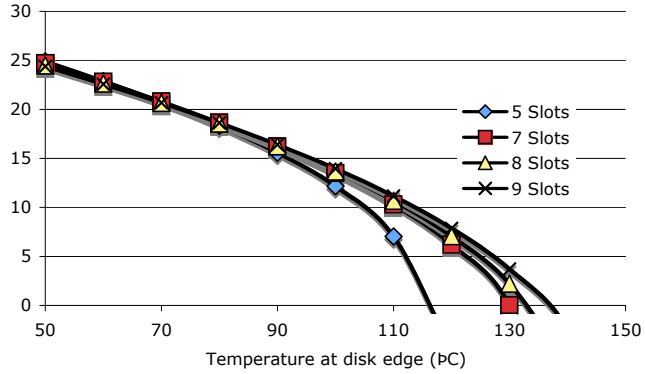

Figure 5-9 Modal Frequency (2 dia., 0 cir.) versus number of slots for threaded saws 5mm thick at 100 rad/s.

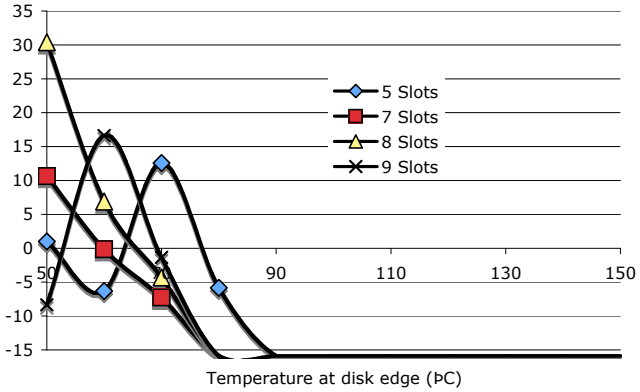

Figure 5-10 Modal Frequency (2 dia., 0 cir.) versus number of slots for threaded saws 3 mm thick at 300 rad/s.

5.4.4 Composite Saw with Inserts

The composite saw with inserts achieved stability numbers similar to that of the threaded saw. Like the threaded saw, the composite saw with inserts also benefits from a higher number of slots due to the higher content of SMA. The results of the composite saw are also comparable to those of the tensioned steel saw. (Figure 5-13)

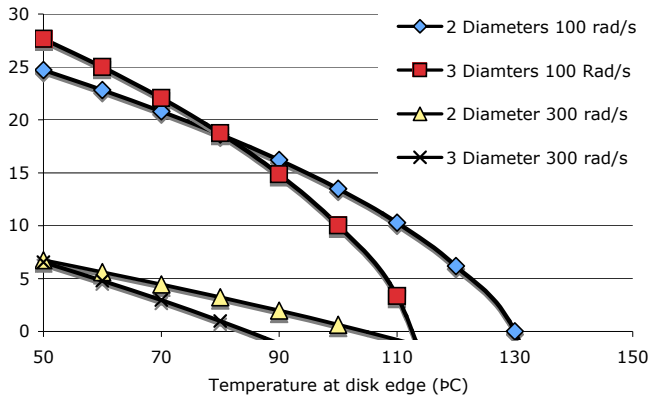

Figure 5-11 5 mm thick composite saw blade with inserts with 7 slots.

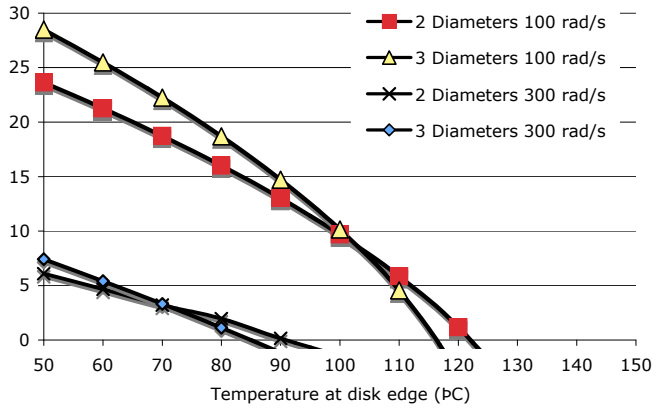

Figure 5-12 5 mm composite saw blade with inserts with 9 slots.

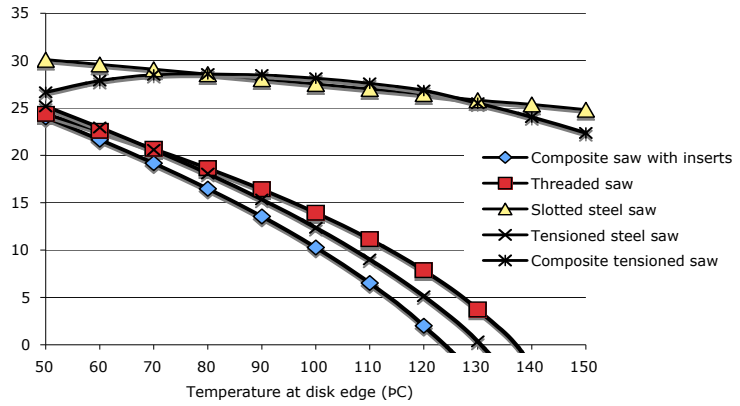

Figure 5-13 Low modal frequencies of 5 mm thick saws at 100 rad/s.

Overall the results of the proposed designs, the threaded saw and the composite saw with inserts are both comparable to those of the tensioned steel saw, commonly used in industry.

5.5 Summary

The natural frequencies of the FEM were compared to those obtained using CSAW, and a strong agreement was found between the two.

The proposed design is to use slots, which are common on saw, and verification showed that the use of slots did not significantly decrease the critical speed of the saw, nor did it increase the amplitude of deflections of the saw.

The proposed design was simulated using the finite element method and compared to the previous ideal design and pretensioned saws. The results showed that the proposed design performed comparably to the pretensioned saws. Ideal saw had higher natural frequencies when heated but was to be expected for the assumptions used in that design. The proposed saw was able to retain its stability over a wider temperature range than the pretensioned saw as predicted.

6 Conclusions

The goal of this thesis was to investigate techniques in which shape memory alloys (SMA) can be used for the purposes of countering instability in the saw due to heating. Through the use of SMA, the investigator hopes to produce a saw with the following benefits:

i. Increased operating speed and temperature.
ii. Decreased kerf.
iii. Decreased thickness of the saw.
iv. Increased range in which the saw is operating in optimum conditions.

These goals were achieved through meeting the follow objectives:

i. Defining the theoretical aspects governing saw design and operation.
ii. Addressing saw design issues including manufacturability, safety, performance and economic viability.
iii. Defining analysis specifications.
iv. Outlining and discussing the simulation results.

Theoretical Aspects

The stability dynamics of a circular saw blade are influenced by disk thickness, rotational speed and temperature. The effect of temperature and rotational speed upon the disk result in stresses within the disk. The thermal stresses has large effect on the saw, including lowering the critical speed. The rotational speed of the saw in operation is limited by its critical speed, and operation of the saw near the critical speed increases saw instability.

Shape memory alloys (SMA) are a class of materials that can exhibit the shape memory effect. It is well suited for uses where a response to heat is sought. The most widely available SMA, nickel titanium (NiTi), is also the one that possesses the strongest shape memory properties. This material is well suited for the proposed design as these properties are present within the operating temperature range of the saw.

Design Issues

A previous design of a disk utilizing SMA demonstrated the ability to increase stability in the disk under rotation while subject to thermal forces. The previous design was developed to one that can satisfy manufacturing, safety, cost, and economic concern through the use of common design methodology.

The safety of the saw was addressed through common risk management. Mitigation techniques such as guarding, automation, avoidance of hazard zones by the operator and proper placement of workstations already greatly reduce safety incidents in sawmill operation. Furthermore, proper engineering design is used to reduce risk of failure. While a proper testing protocol will be establish to mitigate any further risks.

The manufacturability of the saw is addressed through conventional fabrication techniques such as fasteners and mechanical interfaces. Machining techniques used for the proposed design, such as laser or water cutting and grinding, are already in use in the manufacture of circular saws. The production of NiTi is established and standardized process would produce the SMA inserts in an economical fashion.

Proposed techniques of integrating the SMA into the saw include threading, use of mechanical fasteners, composite material of NiTi wire and filament within epoxy, and integration of SMA into the saw through sandwiching between two plates to form a disk. These designs were evaluated used quantitative analysis and it was found that the threaded saw was the best of the proposed designs.

Analysis

To achieve a reliable finite element model for simulation of the design several validation techniques and assumptions were used. The finite element model was refined through comparisons to a commercial saw simulation program, CSAW.

The simulation of the NiTi necessitates the use of temperature dependant properties. For the elasticity, the material's properties are proportional to the composition of austenite and martensite within the material. For the shape memory effect, the material is modeled as having a negative coefficient of thermal expansion. The use of tensioning in the saw is modeled through the application of a thermal stress similar to the actual resultant stresses in a pre-tensioned disk.

Results

The natural frequencies of the FEM were compared to those obtained using CSAW, and a strong agreement was found between the two.

The proposed design is to use slots, which are common on saw, and verification showed that the use of slots did not significantly decrease the critical speed of the saw, nor did it increase the amplitude of deflections of the saw.

The proposed design was simulated using the Finite element method and compared to the previous ideal design and pre-tensioned saws. The results showed that the proposed design performed comparably to the pre-tensioned saws. Ideal saw had higher natural frequencies when heated but was to be expected for the assumptions used in that design.
The proposed saw was able to retain its stability over a wider temperature range than the pre-tensioned saw as predicted.

In other words, the problem of saw blade stability can be simplified to be dependant upon **r**, and the solution can be obtained through the use of the finite difference method to solve Equation 2.12. The addition of inserts and slots to proposed designs, results in non-linear equations and the proposed designs were dependant upon ϕ, making the use of finite element a better choice. The use of temperature profiles to model stresses induced by the SMA proved similar results to experimental testing, and provided for a simpler model.

Through the use of CSAW, the FEA model used was improved for modeling the problem of saw blade stability. This model was then used to design and optimize the integration of saw blade design.

The integration of SMA shows promising performance with the design of the slotted saw. The ideal saw blade showed performance better than the other saws, but the assumptions used in its modeling severely limit its manufacturability. The proposed designs for the saws, the threaded saw and the composite saw with inserts, showed better performance than the standard steel saw and were comparable to the tensioned steel saw. Both these designs provide a basis for the manufacture for testing and optimization purposes. The threaded saw with the use of wire SMA, would be easier to develop due to the greater availability of the material in that form, and the smaller wire being easier to work with.

Although this investigation focused on the problem of saw blade stability similar problems such as refiner plates also provided another avenue to pursue this solution. In the case of refiner plates, stability is also an issue as the plates must operate within close tolerance to one another, but here thickness of the plate is not an issue. The instability brought upon by heating is still present, and the incorporation of SMA could provide a passive mechanism to increase stability. With increased stability, the plates could be run closer together increasing effectiveness, without the risk of plates touching leading to machine downtime and costs associated to plate replacement.

Overall, the results obtained for the threaded saw and the composite insert saw are promising enough to encourage further investigation. The assumptions applied during the simulation are such, that prototyping would be feasible, and is recommended to further research this idea.

7 Nomenclature

a = Radius of clamp. (m)

b = Radius of disk. (m)

c = Intermediate radius on disk. (m)

∇= Del Operator.

d = Ratio of clamp to disk thickness.

d = Diameter of the rivet.

d_1 and d_2 = Constants**.**

Disk=The plate of the saw.

dr = Differential in the radial direction.

$d\phi$ = Differential in the angular direction.

F = Force applied in Newtons.

Gr = Grashof number.

δH = Hight of clamp.

H = ½ thickness of disk.

h_{disk} = Coefficient of convection, disk.

h_{bi} = Modified Biot number.

$h_{cylinder}$= Coefficient of convection, top surface of clamp.

h_{clamp} = Coefficient of convection, side surface of clamp.

I_n = Ordinary Bessel's function of the n kind.

k_f = Conductivity of air.

K_n = Modified Bessel's function of the n kind.

k_{steel} = Conductivity of steel.

kerf = thickness of cut caused during sawing.

n = Number of nodes of vibration.

NiTi= Nickel Titanium = Nitinol™

Nu = Nusselt number : $Nu = \frac{h_{convection} b}{k_{air}}$

ν = Poisson's ratio of kinematic viscosity.

θ = Temperature function for disk.

$\theta_0 = \omega_n$ = Frequency of vibration for nth mode.

θ_0 = Peripheral temperature (T(r) – T_0).

ω_0 = Speed of rotation. (rad/s)

ω_{cr} = Critical speed.

ω_b = Frequency of vibration related to plate stiffness.

ω_m = Frequency of vibration related to membrane stiffness.

OSB= Oriented Strand Board.

Pr = Prandlt number.

p = the distance between rivets.

ϕ= Angular coordinate. (**r**, ϕ, **z** coordinate system).

ϕ_0, = Arbitrary angle position.

$\dot{q}_{in\_conduction}$ = Heat transfer into the control volume by conduction.

$\dot{q}_{in\_cutting}$ = Heat transfer into the control volume by the cutting action.

$\dot{q}_{in\_friction}$ = Heat transfer into the control volume by friction.

$\dot{q}_{out\_conduction}$ = Heat transfer out of the control volume by conduction.

$\dot{q}_{out\_convection}$ = Heat transfer out of the control volume by convection.

$\dot{q}_{out\_sawdust}$ = Heat transfer out of the control volume by heat and mass transfer from the sawdust.

r = Radial coordinate. (**r**, ϕ, **z** coordinate system).

$\mathbf{r_A}$ = Non-dimentional radius a, a/b.

$\mathbf{r_B}$ = Non-dimentional radius b, b/b.

r_c = Transition radius.

Re = Reynolds number.

Sawyer = Saw operator.

SMA = Shape memory alloy.

SME = Shape Memory Effect.

σ_p = Bearing stress.

$\sigma_{t,steel}$ = Tensile stress, steel.

t = Time. (s)

t_0 = Arbitrary time.

τ = Rivet shear stress.

T_0 = 0 °C.

$\mathbf{T_{Af}}$ = Austenite end temperature.

$\mathbf{T_{As}}$ = Austenite start temperature.

$\mathbf{T_{Mf}}$ = Martensite end temperature

$\mathbf{T_{Ms}}$ = Martensite start temperature.

w =Displacement in z direction.

z = z coordinate (**r**, ϕ, **z** coordinate system).

8 Bibliography

Alamgir, A.H.M. Incidence, costs , and compensation of work related injuries among sawmill workers in BC, UBC, August 2006.

Ansys, Ansys 10.0 Documentation, Ansys Inc. 2005.

Brdicko, J. "U.S. Patent # 4567798" United States Patent Office, 1981.

Briggs, J. P., Castaneda, P. P., " Variational Estimates for the Effective Response of Shape Memory Alloy Acutated Fiber Composites," *Transactions of the ASME,* v. 69, July, 2002, pp. 470-480.

Campbell, R. D., *"*High-speed thin-kerf sawing*"*, *Modern Sawmill Techniques V.2*, Feb 1974, pp. 279-292.

Campbell, W. "The Protection of Steam Turbine Disk Wheels from Axial Vibration" *ASME* 46, 1925, pp. 31-160.

D.S. Dugale "Effects of Internal Stress on Elastic Stiffness" *Journal of the Mechanical Physics of Solids,* vol. 11, 1963, pp.41-47.

D.S. Dugale "Effects of Internal Stress on Flexural Stiffness of Discs" *International Journal of Engineering Science,* vol. 1, 1963, pp. 89-100.

D.S. Dugale "Theory of Circular Saw Tensioning" *International Journal of Production Research,* vol. 4, 1966, pp. 237-248.

Demers, Vincent, "Modélisation du compartement des alliage à mémoire de forme sur un logiciel d'élement finis commercial." École de Technologie Supérieure, 2004.

Denig, J., Small Sawmill Handbook: Doing it right and making money, Miller Freeman, 1993.

Eggeler, G., et al., *"Structural and functional fatigue of NiTi shape memory alloys,"* Materials Science and Engineering A, v 378, n, 1-2, 2004, pp. 24-33.

Greenburg, M. Advanced Engineering Mathematics, 2e, Prentice Hall, 1998.

Hodgson, D. et al. *Shape Memory Alloys*, http://www.sma-inc.com/SMAPaper.html, 1999.

Ioras, H., Nicholls, T. Perkins, M.C., " Parametric Modeling of Circular Saws With uniform thickness using Finite Element Analysis", *Journal of the Institute of Wood Science*, vol. 15 issue 1, 2000, pp 28-31.

King, D.H., "Improve your profits through improved recovery" *Modern Sawmill Techniques Proceedings of the Seventh Sawmill Clinic*, March 1977, pp. 105-123.

Kirbach, E. "Testing a New Circular Saw Guide System in a Large Production Sawmill," *Advances in Sawmill Technology,* December 1989, pp. 129-142.

Kostiuk, A.P. and Pleau, J.H., Reduction of Sawdust in Sawmill Operations: Thin-Kerf, Twin Circular Guided Headsaw Pilot Project, Forintek Canada Corp. October, 1994.
Kreith, F. Principles of Heat Transfer, 1978.

Kuratani, F. Yano, S., "Vibration analysis of a circular disk tensioned by rolling using finite element method" *Archive of Applied Mechanics,* v 70, n 4, May, 2000, p 279-288.

Lamb, H. and Southwell, R.V. "The Vibrations of a Spinning Disk" *Proceedings of the Royal Society of London, Series A* Vol. 100, 1921, pp. 272-280.

Lindeburg, M., *Engineer-In-Training Reference Manual 8th Edition*, Professional Publications, 1992.

Mote Jr., C.D. Holoyen, S., "Confirmation of the Critical Speed stability theory for Symmetrical Saws" *Transactions ASME, Series B*, vol. 97, 1975, pp. 1112-1118.

Mote Jr., C.D., "Free Vibrations of Initially Stressed Circular Disks" *Transactions ASME, Series B*, vol. 87, 1965, pp. 258-264.

Mote Jr., C.D., "Theory of Thermal Natural Frequency Variations in Disks" *International Journal of Engineering Science,* vol. 8, 1966, pp. 547-557.

Mote, C.D. Jr., Schajer, G. S., Holoyen, S., "Circular Saw Vibration Control by Induction of Thermal Membrane Stresses", *ASME Journal of Engineering for Industry*, vol 103, 1981, pp. 81-89.

Oberg, E., Jones, F.D., Machinery's Handbook: A Reference Book for the Mechanical Engineer, Draftsman, Toolmaker and Machinist, Industrial Press, 1969.

Otsuka, K., Wayman, C.M. *Shape Memory Alloys*, Cambridge University Press, 1998.

Paro, J.A., et al., "Drilling of conventional cast stainless steel with HIPed NiTi coating," *Journal of Processing Technology*, v. 153-154, 2004, pp. 622-629.

Planning Today for Tomorrow's Future: An energy strategy for British Columbia," British Columbia Energy Council, May 1994.

Poirier, J., *Optimization of Spinning Circular Disk Subject to Peripheral Heating through the use of Shape Memory Alloys,* McGill University, 2003.

Report of task force on sawmill wood residue management, Air Resources Branch, British Columbia Minister of Environment, Lands and Parks, November 2003

Quelch, P. S., Sawmill Feeds and Speeds: Band and Circular Rip Saws, Armstrong Manufacturing Company, 1977.

Schajer, G.S., "CSAW: Guided Circular Saw Vibraion and Stability Program Vers. 3.1", *Wood Machining Institute*, 1995.

Schrooten, J. et al. "Progress on Composites with Embedded Shape Memory Alloys Wires," *Materials Transactions,* Vol. 43, No. 5, 2002, pp. 961-973.

Shackelford, J., *Introduction to Materials Science for Engineers 5th ed*., Prentice Hall, 1999.

Shaw, J. Kyriakides, S. "Thermomechanical Effects of Niti" *Journal of the Mechanical Physics of Science, vol. 43,* 1995, pp. 1243-1281.

Smallman, R.E., Bishop, R.J., Modern Physical Metallurgy and Materials Engineering: Science, Process, Applications, Butterworth-Heinemann, 1999.

Southwell, R.V. "On the Free Transverse Vibrations of a Uniform Circular Disk Clamped at its Center; and on the effects of Rotation" The Vibrations of a Spinning Disk" *Proceedings of the Royal Society of London, Series A* Vol. 101, 1922, pp. 133-153.

Stakhiev, Y. M., "Coordination of saw blade tensioning with rotation speed", *Holz als Roh- und Werkst*, vol. 62, 2004 pp. 313-315.

Stakhiev, Y. M., "Research of circular saw roll tensioning in Russia: Practical adjustment methods", *Holz als Roh- und Werkstoff*, vol. 57, 1999 pp. 57-62.

Stakhiev, Y. M., "Research on circular saw disc problems: several of results", *Holz als Roh- und Werkstoff,* vol. 61, 2003 pp. 13-22.

Sun, C.T., *Mechanics of Aircraft Structures*, John Wiley & Sons, 2006.

Szymani, "Status Report on the technology of saws." *Forest Products Journal,* v.36, n. 4, 1986, pp 15-19.

Szymani, R. "Latest Developments in Circular Saw Testing." *Forest Products Journal*, v 34, n 5, May, 1984, p 64-68.

Szymani, R. and C.D. Mote Jr. "Principle Developments in Thin Saw Vibration and Control Research Part 2: Reduction and Control of Saw Vibration" *Holz als Roh-und Werstoff,* vol 35. 1977 pp. 219-225.

Szymani, R. and C.D. Mote Jr. "Principle Developments in Thin Saw Vibration and Control Research Part 1: Vibration of Circular Saws" *Holz als Roh-und Werstoff,* vol 35. 1977 pp. 189-196.

Szymani, R., Mote, C.D. Jr., "Circular Saw Stiffness as a Measure of Tension," *Forest Products Journal,* v. 27, n. 3, 1977, pp. 28-32.

Thrasher, Al, "Saw Lumber: Not Sawdust," *Modern Sawmill Techniques Proceedings of the Seventh Sawmill Clinic*, March 1977, pp. 105-123.

Timoshanko. S., Lessells, J.M. *Applied Elasticity,* 1925.

Tobias. S.A., Arnold, R.N. "The Influence of Imperfection on the Vibration of Rotating Disks", *Proceedings of the Institution of Mechanical Engineers*, vol. 171, 1957, pp. 669-690.

Vogel, M., Skinner, D.W. “Natural Frequencies of Transversely Vibrating Uniform Annular Plate” *Transactions ASME, Series E*, vol. 87, 1965, pp. 547-557.

Wang, Ge, “Welding of Nitinol to Stainless Steel,” SMT Proceedings of the 2nd International Conference on Shape Memory and Superelastic Technologies, 1997, pp. 131-136.

Williston, E., Lumber Manufacturing: The design and operation of sawmills and planer mills, Forest Products Society, 1988.

Xiaochin, G. W., Sun, J. C., “Active Sensing and Control of Vibration of Circular Saws – A Comparison of Optimal and Variable Structure Control”, *Proceedings of the American Control Conference,* 2001, pp. 4294-4299.

Zhonge, B., et al., “ Material Characterization of SMA Actuators under Non-Proportional Thermomechanical Loading”, *Journal of Engineering Materials and Technology,* v. 121, n. 1, pp. 75-85.

Zienkiewicz, O. C., Taylor, R. L., *The Finite Element Method, vol. 1: The Basis,* Butterworth-Heinemann, 2000.